Development of a multiphase chemical mechanism to improve secondary organic aerosol formation in CAABA/MECCA (version 4.5.6-rc.1)

Felix Wieser[1], Rolf Sander[2], Changmin Cho[1,a], Anna Novelli[1], Hendrik Fuchs[3], Ralf Tillmann[1], Thorsten Hohaus[1], and Domenico Taraborrelli[1]

[1]Forschungszentrum Jülich GmbH, Institute of Energy and Climate Research, IEK-8: Troposphere, Jülich, Germany
[2]Atmospheric Chemistry Department, Max Planck Institute for Chemistry, Mainz, Germany
[3]Department of Physics, University of Cologne, Cologne, Germany
[a]Now at: Atmospheric Chemistry Observations and Modeling Laboratory, National Center for Atmospheric Research, Boulder, USA

Correspondence: Felix Wieser (f.wieser@fz-juelich.de) and Domenico Taraborrelli (d.taraborrelli@fz-juelich.de)

Abstract. During the last decades, the impact of multiphase chemistry on secondary organic aerosol (SOA) has been demonstrated to be key in explaining ~~lab~~ laboratory experiments and field measurements. However, global atmospheric models still show large biases when simulating atmospheric observations of organic aerosols (OA). Major reasons for the model errors are the use of simplified chemistry schemes of gas-phase oxidation of vapors and parameterization of heterogeneous surface reactions. The photochemical oxidation of anthropogenic and biogenic volatile organic compounds (~~VOC~~VOCs) leads to products that either produce new SOA or are taken up by existing aqueous media like cloud droplets and deliquescent aerosols. After partitioning, aqueous-phase processing results in polyols, organosulfates, and other products with a high molar mass and oxygen content. In this work, we have introduced the formation of new low-volatility organic compounds (~~LVOC~~LVOCs) into the multiphase chemistry box model CAABA/MECCA. Most notable ~~is the addition~~ are the additions of the SOA precursors limonene, n-alkanes (5 to 8 C atoms), and a semi-explicit chemical mechanism for the formation of ~~LVOC~~ LVOCs from isoprene oxidation in the gas- and aqueous-phase. Moreover, Henry's law solubility constants and their temperature dependences have been estimated for the partitioning of organic molecules to the aqueous-phase. Box model simulations indicate that the new chemical scheme predicts enhanced formation of ~~LVOC~~LVOCs, which are accounted for being precursor species to SOA. As expected, the model predicts that ~~LVOC~~ LVOCs are positively correlated to temperature but negatively correlated to NO_x levels. However, the aqueous-phase processing of isoprene-epoxydiols (IEPOX) displays a more complex dependence on these two key variables. Semi-quantitative comparison with observations from the SOAS campaign suggests that the model may overestimate methylbutane-1,2,3,4-tetrol (MeBuTETROL) from IEPOX. Further application of the mechanism in the modeling of two chamber experiments (limonene-ozone and isoprene-NO_3) shows a sufficient agreement to experimental results within model limitations. The extensions in CAABA/MECCA will be ~~ported~~ transferred to the 3D-atmospheric model MESSy for a comprehensive evaluation of the impact of ~~aqueous-phase~~ aqueous-/aerosol-phase chemistry on SOA at a global scale in a follow up study.

1 Introduction

Secondary organic aerosol (SOA) is formed from anthropogenic and biogenic ~~VOC~~ volatile organic compounds (VOCs) in the atmosphere and comprises a significant amount of the total ~~OA~~ organic aerosol (OA) mass (Hallquist et al., 2009). Atmospheric aerosols have received increased attention in recent years, as a result of their impact on human health, urban visibility, and climate change ~~(Lin et al., 2017; Chen et al., 2020; Zhong and Jang, 2011; Zhu et al., 2017)~~(Zhong and Jang, 2011; Zhu et al., 2017; Lin et a . New SOA precursors, formation pathways, and loss reactions in the gas- and the aqueous-phase have been discovered ~~(Wennberg et al., 2018; Hodzic et al., 2014; Lim et al., 2010)~~(Lim et al., 2010; Hodzic et al., 2014; Wennberg et al., 2018). In current models, aqueous-phase pathways leading to SOA are continuously improved, as their importance has been demonstrated in experiments ~~(Lin et al., 2014; Carlton et al., 2007; Ervens, 2015)~~(Carlton et al., 2007; Lin et al., 2014; Ervens, 2015) . Hu et al. (2015) investigated aqueous SOA (aqSOA) tracers from isoprene oxidation and found a contribution between 6 % and 36 % to total OA.

~~Model results display~~ Recent models show different biases in ~~recent models~~their results. Traditional global models generally underestimate SOA mass, especially during haze events, due to the increase in pollutant concentrations (Heald et al., 2011; Tilmes et al., 2019). This gap between models and observations is continuously decreasing in recent years, but SOA formed in available aqueous-phase is often still neglected (Shrivastava et al., 2017). Aqueous SOA is known to be more oxidized than SOA formed from gas-phase precursors, thus the modeled O/C ratios commonly do not match experimental results (Lim et al., 2010). Additionally, products from aqueous-phase oxidation are formed on different time-scales than from gas-phase oxidation. Combined with aqueous- and gas-phase properties (pollutants, pH), this impacts the vertical distribution of SOA in the atmosphere depending on the simulation setup (Seinfeld and Pandis, 2016; Hodzic et al., 2016).

We have implemented recent experimental results and formerly neglected SOA precursors into the chemistry scheme of the box model CAABA/MECCA. The updated chemical mechanism is meant to be used for further advancing global simulations of SOA with the EMAC model (Pozzer et al., 2022). EMAC is the global configuration of the Modular Earth Submodel System (MESSy) ~~(Jöckel et al., 2006; Kerkweg et al., 2007; Tost et al., 2006; Jöckel et al., 2010, 2016)~~(Jöckel et al., 2006; Tost et al., 2006; Kerky . This approach has two advantages: 1) model simulations in the test phase are considerably faster in the box than in the global model; 2) thanks to the MESSy interface structure, the MECCA chemical mechanism can directly be used in the global model EMAC. This allows us to be fast in the implementation process while being able to use the new chemistry in the global model without further adaptations. The partitioning to the aqueous-/particle-phase plays an important role in the SOA formation process. As temperature-dependent Henry's law solubility constants (H_s) for large organic molecules are sparse in the literature, these properties have to be estimated. The corresponding approach is discussed in Sect. 2.4. In Section 3 the new chemical scheme is evaluate against model, observational, and chamber data. In the following section, we introduce major specifications of the CAABA/MECCA model.

2 Model description

2.1 Specifications

CAABA/MECCA is a combination of the box model CAABA (Chemistry As A Box model Application) and the atmospheric chemistry model MECCA (Module Efficiently Calculating the Chemistry of the Atmosphere) (Sander et al., 2019). The chemistry module MECCA is also used in the global model EMAC, simplifying the adoption of box model changes into the global model. MECCA contains both gas- and aqueous-phase chemistry and the species can partition between the phases. Simulations with solely gas-phase are also possible to simulate dry conditions. For the partitioning, Henry's law solubility constants are utilized. Non-linear effects like "salting in" and "salting out" influence Henry's law solubility constants. It has been shown that the partitioning of compounds can be substantially influenced by the aerosol salt concentration (Kampf et al., 2013; Herrmann et al., 2015). Similarly, aqueous-phase reaction rates can be influenced by salt composition (Mekic and Gligorovski, 2021). The model does not account for these effects, due to the insufficient data availability ~~(Sander, 2015)~~ (Sander, 2023). This may result in partially incorrect partitioning rates.

Available mechanisms for organic chemistry are the Mainz Organic Mechanism (MOM) (Sander et al., 2019) and the Jülich Aqueous-phase Mechanism of Organic Chemistry (JAMOC) by Rosanka et al. (2021). MOM is the default oxidation mechanism of ~~VOC~~ VOCs in MECCA. It contains an advanced treatment of chemistry of isoprene (Taraborrelli et al., 2012; Nölscher et al., 2014; Novelli et al., 2020), monoterpenes (Hens et al., 2014; Mallik et al., 2018) and aromatics (Cabrera-Perez et al., 2016; Taraborrelli et al., 2021). JAMOC is a reduced subset of the CLEPS mechanism (Mouchel-Vallon et al., 2017). Although built for global chemistry simulations, both chemical mechanisms together cover a wide range of reactions. Combined, they include gas-phase oxidation and gas/aqueous partitioning for species up to 11 carbons and aqueous-phase oxidation for species up to ~~4~~ four carbons. The submodel JVAL calculates photochemical rate constants (j values) based on cross-sections and quantum yields (Sander et al., 2014). The related j values are usually first determined for the smallest compound of a compound class and this value is applied to higher homologs. For instance, j values for the photolysis of all organic hydroperoxides are taken equal to the one for methyl hydroperoxide ($j_{\mathrm{CH_3OOH}}$). This is also done in the Master Chemical Mechanism (MCM) (Jenkin et al., 1997). More details about CAABA/MECCA can be found elsewhere (Sander et al., 2005, 2011, 2019).

2.2 Model limitations

The main goal of the CAABA/MECCA box model is the investigation of chemical reaction mechanisms in the atmosphere. Other processes (e.g., dynamics and microphysics) are simplified or neglected. Specifically, formation and loss of SOA are not included. Cloud droplets and rain were not modeled, and therefore no scavenging or wet deposition. LVOCs can dissolve and react in deliquescent (aqueous) aerosols but not in an organic apolar medium. We chose CAABA/MECCA regardless of the mentioned limitations, as this study is intended to present the chemistry scheme and demonstrate the possible influence of the update on future results. We applied the following assumptions to display the ability of the chemical mechanism to simulate experimental/observational results. Generally, we assume low-volatile organic compounds (LVOCs) as a proxy for SOA, disregarding the partitioning process. To model isoprene observation, LVOCs is defined as compounds that exhibits

an H_s larger than 10^8 M/atm (see Sect. 3.1.1). For the limonene-ozone experiment, a lower H_s threshold of 4×10^6 M/atm was selected. This rule is applied to species in the gas- and the aqueous-phase, to tackle the missing condensation and new particle formation. Different thresholds were chosen, due to varying conditions affecting the importance of condensation and new particle formation and the molar mass of the major SOA products. Limonene products are more likely to condense on preexisting aerosols due to their lower saturation vapor pressure.

We intend to give an advanced evaluation of the presented mechanisms in the global model EMAC with a further extended mechanism. Due to the wide range of available submodules solving most of the above-mentioned limitations (Tost et al., 2006; Pringle et al. , EMAC can give a more in-depth analysis of the impact of the mechanism and advances needed in future updates.

2.3 Mechanism development

2.3.1 Overview

Table 1 lists the newly implemented and updated precursors, split into biogenic and anthropogenic ~~origination~~origin. A major update to the ~~chemistry~~ chemical mechanism is introduced by updating the isoprene oxidation scheme. Additionally, the β-pinene and benzene ~~mechanism~~ mechanisms are revised. Limonene, IEPOX and ~~long chain alkane~~ n-alkane mechanisms were newly added. The chemistry schemes of the monoterpenes sabinene, camphene, and carene had been based on α-pinene and were not developed for the individual compounds. They are ~~now~~ currently excluded as they do not fulfill the standard of the implemented chemistry and will potentially be reintroduced with a more refined mechanism. The impact of these monoterpenes on ~~LVOC~~ LVOCs in the forward analysis is small, as depicted in fig. S9 in the supplement. In the following sections, changes to the specific mechanisms are described in detail.

2.3.2 Gas-phase kinetics

The nitrate radical addition to isoprene is improved based on Vereecken et al. (2021), which has been validated against chamber experiments (Carlsson et al., 2023). ~~Similar products as in the~~ The former oxidation mechanism ~~are formed, while product yields are redistributed~~in MECCA is substituted by new pathways and products, including epoxide formation. The resulting mechanism represents a subset of the original scheme by Vereecken et al. (2021). Isoprene OH-oxidation under low NO_x-conditions is revised by adding the formation of epoxydiols (IEPOX) according to St. Clair et al. (2016) and dihydroxy hydroperoxy epoxides (ISOPBEPX) according to D'Ambro et al. (2017). Both compounds were previously identified as main SOA precursors (Lopez-Hilfiker et al., 2016; D'Ambro et al., 2017). Furthermore, the gas-phase oxidation of IEPOX as described by Bates et al. (2014) is included in the new mechanism. The monoterpenes α-pinene and β-pinene are already included in the MECCA scheme with a refined mechanism. To simulate a wide range of monoterpenes, the oxidation of limonene was added to the model. The update is based on the chemical scheme of the Master Chemical Mechanism (MCM v3.3.1) by Jenkin et al. (1997) (http://mcm.york.ac.uk). If available, reaction rates are re-calculated by structure-activity relationships (SARs), and low-yield pathways are excluded. Furthermore, the mechanism was refined by results of Carslaw (2013) and Vereecken and Peeters (2012). ~~Products important for~~ Branching ratios of the limonene-ozone mechanism were adapted by Pang et al. (2022)

Table 1. List of all newly implemented and updated ~~species~~VOC, together with the main reactants and main mechanism sources. Compounds are divided into biogenic and anthropogenic ~~origination~~origin.

Precursor	Implementation type	Main reactant	Mechanism sources
Biogenic			
isoprene	update	NO_3	Vereecken et al. (2021)
isoprene	update	OH	St. Clair et al. (2016), Bates et al. (2014) D'Ambro et al. (2017)
IEPOX	new	OH	Petters et al. (2021), Riedel et al. (2016)
limonene	new	OH / ozone / NO_3	MCM, Pang et al. (2022), Carslaw (2013), Vereecken and Peeters (2012)
β-pinene	update	OH	Vereecken and Peeters (2012)
sabinene / carene / camphene	excluded	OH / ozone	
Anthropogenic			
benzene	update	OH	Xu et al. (2020), Wang et al. (2013)
pentane, hexane, heptane, octane	new	OH	Sivaramakrishnan and Michael (2009) Atkinson et al. (2008)

. Products important to SOA are highly oxidized large hydroperoxides and ketones. Small adjustments referring to Vereecken and Peeters (2012) were introduced for β-pinene.

Anthropogenic SOA precursors are represented by aromatics and ~~large~~ n-alkanes. The oxidation scheme of benzene and toluene is rather detailed in the model, while higher substituted aromatics are treated in a simplified manner (Cabrera-Perez et al., 2016; Taraborrelli et al., 2021). Benzene chemistry is updated according to the results by Xu et al. (2020) who found no evidence for the epoxide channel. ~~We distribute~~ This was validated by previous theoretical work by Vereecken (2019) . We distribute the epoxide production into competing pathways (see Fig. S7). This adaptation yields more small, oxidized compounds like glyoxal. Thus a decrease in SOA mass in absence of cloud processing and efficient oligomer formation is expected. Similar changes for the epoxide channel were found for the OH oxidation of toluene, but at the same time the formation of alternate epoxides was shown ~~(Zaytsev et al., 2019; Wu et al., 2014)~~(Wu et al., 2014; Zaytsev et al., 2019). MOM treats the oxidation of alkanes up to 4 carbons. Based on the field measurements of McDonald et al. (2018), the mechanism has been extended for n-alkanes with sizable emissions (up to n-octane). The n-alkane mechanism is based on the work of Atkinson et al. (2008) and yields hydroperoxides, alkyl nitrates, and organic molecules containing ketone and hydroxyl groups. This mechanism is simplified and thus only covers the oxidation of specific reaction sites, and only one H-abstraction process is considered.

Experimental studies have shown partitioning of multifunctional alkyl nitrates to the aerosol phase (Perring et al., 2013). The yields of alkyl nitrates from the new $RO_2 + NO$ reactions for limonene and n-alkanes are implemented following the protocol by Sander et al. (2019). These yields depend on the number of heavy atoms, temperature, and pressure (Arey et al., 2001; Teng

et al., 2015). Thus, the updated model is expected to generate significant amounts of SOA precursors over continental polluted regions during wintertime.

The rate constants for common reactions (e.g., OH-addition and H-abstraction) are taken from predefined functions implemented in MECCA, while rate constants for specific reactions are taken from the literature or are calculated by SAR (Kwok and Atkinson, 1995; Sander et al., 2019). In the isoprene and limonene mechanisms we consider H-shifts in peroxy radicals as described and estimated by Vereecken and Nozière (2020). In this scheme, the H-shift depends on neighboring substituents, yielding mainly highly oxygenated molecules (HOMs). New hydroperoxides either react with OH radicals by H-abstraction to reform the corresponding peroxy radical or decompose into an alkoxy and an OH radical. The decomposition step is mainly applied to molecules with neighbouring reactive groups, e.g., double bonds, which show a high reactivity towards alkoxy radicals, yielding epoxides. This kinetic scheme is key to the IEPOX and ISOPBEPX formation. In the alkane oxidation mechanism alkoxy radicals mainly undergo 1,5-H-shifts. Graphical representations of main pathways of all new reaction mechanisms are shown in Figs. S1-S8 in the supplement.

2.3.3 Aqueous-phase kinetics

Rate constants and branching ratios in the aqueous-phase are taken from Mouchel-Vallon et al. (2017), if available. Similar to the CLEPS 1.0 protocol, H-abstractions by hydroxyl radicals are estimated with the SAR by Monod and Doussin (2008). Only the fastest H-abstraction pathways are considered, even though the SAR provides branching ratios for the different reactive sites. The examination of all CH-bonds would require a general aqueous-phase C-H abstraction scheme in MECCA for all generated products, which is not included in the present model.

Kinetics of the IEPOX reactive uptake (acid catalyzed ~~ring opening~~ring-opening) are taken from the supplementary information of Petters et al. (2021), while the branching ratios are extracted from Riedel et al. (2016). In a moderately polluted atmosphere, methylbutane-1,2,3,4-tetrol (MeBuTETROL) is the main product of aqueous IEPOX oxidation, while the corresponding organosulfate is dominant in the presence of sulfate aerosols. As an addition to the production scheme, we developed and implemented a loss mechanism based on Cope et al. (2021), which we similarly applied to ISOPBEPX. Cope et al. (2021) revealed formic acid as the main oxidation product. They proposed a mechanism, explaining the formic acid formation, invoking some reactions to proceed at unusual rates in aqueous media. Figure 1 shows our adapted and revised mechanism. Comparing the typical rate constants of the possible pathways, we redistributed the oxygen abstraction by NO to the HO_2 elimination. The latter is nevertheless consistent with the observed formic acid yield. Similar to the mechanism by Cope et al. (2021), Fig. 1 displays the abstraction of the hydrogen atom at C4 in the mechanism. In addition, we have implemented the abstraction of the hydrogen atom at C1 after the HO_2 elimination yielding hydroxyacetone (not shown). Oxidation of the latter leads to the formation of the geminal diol of methyl glyoxal. The simplest geminal diol, from hydration of formaldehyde, has been shown to efficiently form formic acid by oxidation in both gas- and aqueous-phase (Franco et al., 2021). Similarly, the geminal diol of methylglyoxal yields formic acid directly but also indirectly via pyruvic acid. The related chemistry is already available in JAMOC (Rosanka et al., 2021).

~~Simplified MeBuTETROL aqueous-phase oxidation mechanism by Cope et al. compared to the mechanism applied in MECCA. The mechanism is similarly applied for ISOPBEPX. Aqueous-phase production of formic acid is via oxidation of the geminal diol of methylglyoxal (not shown). The H-abstraction at the red hydrogen (C1; assumed to be 50) yields additional formic acid.~~

As an update to earlier work, we have introduced the hydrolysis of organic nitrates in the aqueous-phase, formed from the gas-phase oxidation of isoprene with OH after NO addition (Vasquez et al., 2020). Similar to the small adaptation to the isoprene NO_3 mechanism, we introduce the outgassing of the oligomers of glyoxal and methyl glyoxal as an update to the JAMOC mechanism. The applied H_s values can be found in Table S2 in the supplement.

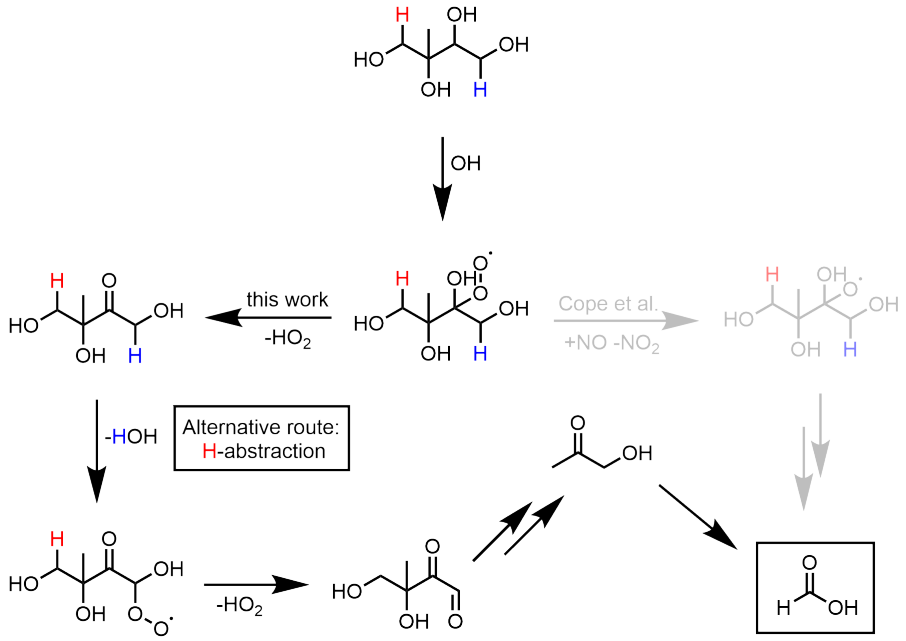

Figure 1. Simplified MeBuTETROL aqueous-phase oxidation mechanism by Cope et al. compared to the mechanism applied in MECCA. The mechanism is similarly applied for ISOPBEPX. Aqueous-phase production of formic acid is via oxidation of the geminal diol of methylglyoxal (not shown). The H-abstraction at the red hydrogen (C1; assumed to be 50%) yields additional formic acid.

2.4 Phase partitioning

2.4.1 Henry's law solubility constants

Henry's law describes the partitioning of a compound between the gas- and the aqueous-phase. In MECCA, Henry's law solubility constants H_s are defined as

$$H_s = \lim_{c \to 0} c/p \tag{1}$$

where c and p are the equilibrium concentration and partial pressure of the compound, respectively. Most values are taken from the compilation by ~~Sander (2015)~~Sander (2023). However, for many species, especially for reaction intermediates, data are not available. Therefore, an estimation method is required. Different approaches are available. The most widely used procedures are HenryWIN and GROMHE. HenryWIN is developed and contributed by the US environmental protection agency (US-EPA, 2012). It estimates Henry's law solubility constants based on molecular structure descriptors (bond contribution) (Meylan and Howard, 1991). The training set consists of 345 species with additional 90 chemicals for subsequent regression and results are validated with 72 compounds. The second Henry's law solubility constant estimation method, called GROMHE, is based on a group contribution approach. Similar to HenryWIN, the estimation is executed by multiple linear regression (Raventos-Duran et al., 2010). It uses a training set of 345 species and a validation set of 143 chemicals. Raventos-Duran et al. (2010) compared both methods and concluded that both show higher uncertainties for increasing solubilities. They revealed a large error for multifunctional compounds in HenryWIN using the GROMHE validation set. H_s are overestimated for difunctional molecules, while compounds with more than two functional groups are underestimated in HenryWIN. However, running HenryWIN with the training set of GROMHE led to increased precision of the HenryWIN prediction.

Figure 2 displays the estimated Henry's law solubility constants by GROMHE and HenryWIN for the closed-shelled compounds of the newly implemented limonene mechanism. The diagram displays a good agreement between the two methods for a vast majority of the estimations, while a small subset shows a high deviation. 61% of all values lie within an order of magnitude. Larger prediction differences have a smaller impact on compounds with a generally high H_s, as these will partition nearly completely to the aqueous-phase in both cases. At low to medium H_s the compounds which are higher estimated by GROMHE have multiple functional groups, containing mainly hydroxyl and carbonyl groups. Compounds predicted to be more soluble by HenryWIN mostly contain nitrate groups, together with further functional groups containing oxygen. A comparison to COSMOtherm values from Wang et al. (2017) does not support either of the estimation methods but lies generally in between the predictions. We use H_s estimated by GROMHE. We chose GROMHE over HenryWIN because it contains a larger default training set and a better performance towards multi-functional molecules. New H_s were included for compounds contained in the update. Already implemented H_s were not changed.

2.4.2 Temperature dependence

The van't Hoff equation describes the temperature dependence of equilibrium constants based on enthalpy. We apply it to Henry's law and define the temperature-dependence factor B as

$$B = \frac{\mathrm{d}\ln H_\mathrm{s}}{\mathrm{d}(1/T)} = \frac{-\Delta_\mathrm{sol}H}{R}, \tag{2}$$

where $\Delta_\mathrm{sol}H$ is the enthalpy of dissolution, and R is the gas constant. The substance-specific value of B is often not known, in particular for large or highly-oxidized compounds. Since it can impact the partitioning considerably, it has to be estimated. Kühne et al. (2005) present an estimation approach for B, based on the linear combination of B(X) values for predefined molecular fragments, resulting in the final value of B. These fragments can be single atoms (e.g., carbon in the chain) or full functional and larger groups (e.g., hydroxyl groups). Unfortunately, the hydroperoxide moiety has not been included as

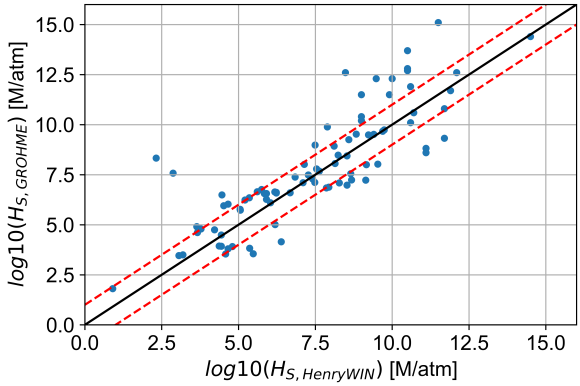

Figure 2. Comparison of H_s estimations by GROMHE and HenryWIN for the newly implemented limonene mechanism. Both axis have a logarithmic scale. The black line represents a one-to-one comparison between both methods. The red doted lines show a deviation of one order of magnitude.

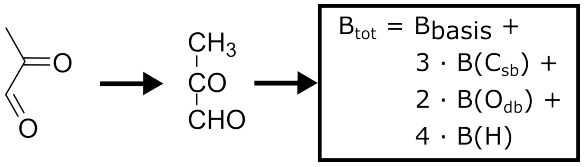

Figure 3. Example for the estimation of the temperature-dependence factor B for Henry's law solubility constant of methylglyoxal. The subscript 'sb' denotes a single and 'db' a double bond.

a molecular fragment by Kühne et al. (2005). As it plays an important role in this study, we have estimated B(OOH) as the difference between B(ethane) and B(ethyl hydroperoxide). The B(X) factors used in this study are shown in Tab. 2. As an example, Fig. 3 illustrates the calculation of B(methylglyoxal).

The method assumes that B(X) values for different fragments are additive and that the contribution of a molecular fragment is the same for every molecule it is attached to. To compensate for this, Kühne et al. (2005) introduce correction factors for specific molecular structures that can be applied to the calculated B after estimation. The relevant correction factors for molecules included in the update are listed in Tab. 2. Figure 4 shows estimated values of B compared to literature data. While most molecules are predicted within one order of magnitude, a tendency to overprediction can be observed for some compounds. The outliers are mainly comprised of multi-functional molecules that are affected by correction factors, implying that the corrections are not strong enough to achieve fitting values. Nevertheless, this approach reflects the trend indicated by the data from ~~Sander (2015)~~ Sander (2023) and Kühne et al. (2005). This estimation approach could be adjusted using additional and stronger correction factors reflecting ~~more~~ better the measured values. Note that B is defined differently in this work and in Kühne et al. (2005). For a direct comparison, a conversion of B is necessary (see Table 2).

Table 2. B-values of group contribution and correction factors for the estimation of the temperature-dependent Henry's law solubility constants. All fragments and B-values, except for the hydroperoxy fragment, are taken from Kühne et al. (2005) and converted referring to our Henry's law solubility constant definition (multiplied by $\ln(10)$). The correction factors containing hydroxyl groups are similarly applied for hydroperoxides. The correction fragment name describes the corresponding structure in SMILES notation.

Fragment	**B-factor / [K]**
basis	1202
Csb / single bond	-60
Cdb / double bond	541
H	203
OH	4145
O / double bond	2931
-O-	1966
ONO2	-811
OOH	3625
correction factors	
C(=O)CO	-1538
COCCO	-1538
COC(OO)	-1538
C(=O)O	-3009
C(=O)OO	-3009

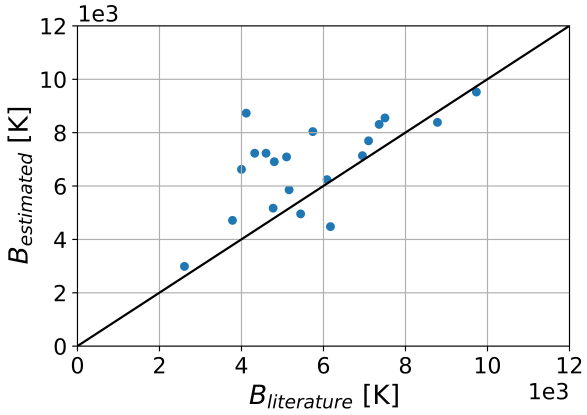

Figure 4. Comparison of estimated vs literature temperature dependence factor B of Henry's law solubility constants. Literature data are extracted from ~~Sander (2015)~~ Sander (2023) and Kühne et al. (2005).

Figure 5 shows temperature-dependent Henry's law solubility constants H_s for alcohols and aldehydes between 270 K and 300 K. Estimated H_s reasonably agree with experimental values in case of the alcohols. The aldehydes display a stronger

divergence. This might be due to hydration of the aldehydes in aqueous media, or similar interactions, for which the estimation is not corrected for. Nevertheless, Fig. 5 also illustrates the need for temperature-dependent H_s, as the constants vary over one order of magnitude. This effect is found to be more pronounced for compounds containing multiple functional groups, as more molecular fractions with high B values are applied (see Tab. S2). B values were added to the model for all H_s without available temperature dependency.

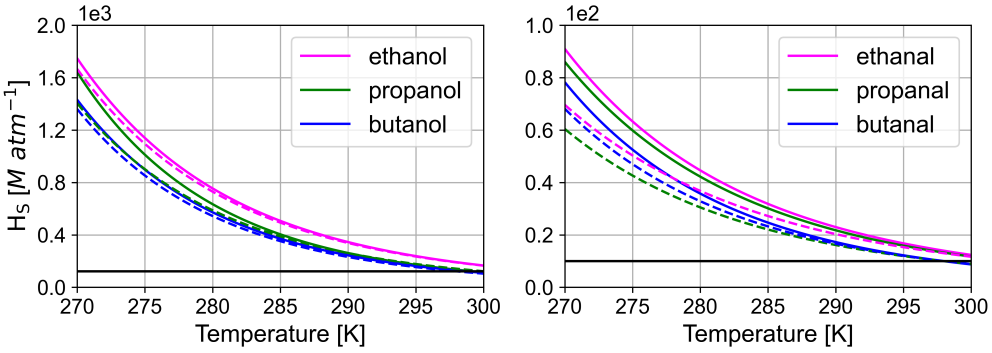

Figure 5. Comparison between estimated and experimental H_s as a function of temperature. Solid lines denote experimental and dashed lines estimated values. The black solid line denotes H_s at 298 K with no further temperature correction. Experimental data are taken from Staudinger and Roberts (2001).

3 Results and discussion

3.1 ~~Model parameters/initialization~~Model-model and model-observation comparison

3.1.1 Model parameters/initialization

We have evaluated potential impacts of the new mechanism ~~under varying conditions~~ on model simulations by comparison to the old mechanism and in modeling IEPOX observations of the Southern Oxidant and Aerosol Study (SOAS). Model conditions are adapted to conditions during the SOAS campaign. Further details of the SOAS campaign are given elsewhere (Budisulistiorini et al., 2015; Ayres et al., 2015; Sareen et al., 2016). Table 4 displays the initial mixing ratios used in all model runs in Sect. 3.1, unless mentioned otherwise. The mixing ratio of isoprene has been fixed to 4 $\mathrm{nmol/mol}$, which is the average measured during the ~~Southern Oxidant and Aerosol Study (SOAS)~~SOAS campaign (Hu et al., 2015). For the same reason, the average aerosol salt composition during the SOAS campaign is adopted (Xu et al., 2015b) ~~. This~~ (see Tab. 3). The SOAS scenario is representative of a mildly polluted deciduous forest during summertime. All simulations are executed for a full diurnal cycle. The sensitivity runs are summarized in Tab. 5.

Table 3. Aerosol properties: Chemical composition, liquid water content (LWC) and particle radius. The chemical composition is averaged from Xu et al. (2015b). The LWC is taken from Nguyen et al. (2014). The average ambient temperature ($T_{ambient,SOAS}$) and particle liquid water temperature ($T_{aerosol,SOAS}$) is given to provide a better comparison between the model and observations (You et al., 2014; Nguyen et al., 2014).

Chemical composition						
NH_4^+ / $\frac{\mu g}{m^3}$	NO_3^- / $\frac{\mu g}{m^3}$	SO_4^{2-} / $\frac{\mu g}{m^3}$	LWC / $\frac{\mu g}{m^3}$	$r_{aerosol}$ / µm	$T_{ambient,SOAS}$ / K	$T_{aerosol,SOAS}$ / K
0.9	0.7	2.4	3.0	1.0	295.2-301.2	300.6

Table 4. Initial mixing ratios for all model runs. Values for NO and ~~NO_2~~ NO_2 are adapted to low, medium and high emissions in Sect. 3.1.1. The mixing ratios of ~~O_2~~ O_2, ~~N_2~~ N_2, ~~CO_2~~ CO_2 and isoprene (C_5H_8) are fixed.

Species	mixing ratio / [nmol/mol]	Species	mixing ratio / [nmol/mol]
H_2O_2	7	MGLYOX	0.5
O_3	25	C_5H_8	4
O_2	2.1×10^{8}	PAN	0.1
NH_3	1	NO_3	3.15×10^{-3}
NO	2×10^{-2}	APINENE	0.6
NO_2	4×10^{-2}	BPINENE	0.6
HNO_3	5×10^{-3}	HCOOH	0.35
N_2	7.8×10^{8}	LIMONENE	0.6
CH_4	1.86×10^{3}	BENZENE	0.1
HCHO	5	ACETOL	4
CO	100	C_5H_{12}	0.4
CO_2	3.5×10^{5}	C_6H_{14}	0.4
CH_3CO_2H	2	C_7H_{16}	0.4
CH_3CO_3H	1.5	C_8H_{18}	0.4
CH_3OH	0.5	CH_3OOH	4
HONO	4×10^{-5}	TOLUENE	0.1

3.2 ~~BASE vs OLD run~~

3.1.1 BASE vs OLD run

The CAABA/MECCA box model does not simulate the production of SOA particles. Yet, a first assessment of the impact of the newly added chemistry on SOA precursors can be done by analyzing low-volatility organic compounds ~~(LVOC)~~ which can act as SOA precursors. Thus, we analyze the total (gas, aqueous and aerosol) mixing ratios of implemented ~~LVOC~~LVOCs. In the scope of this analysis, ~~LVOC~~ LVOCs are defined as ~~VOC~~ VOCs fulfilling the condition $H_s > 10^8\,\mathrm{M/atm}$, following

Table 5. Abbreviation and description of the different setups for the sensitivity runs.

Abbreviation	Description
BASE	base run with the updated mechanism
OLD	model run with CAABA/MECCA 4.5.5
BASE-278K	low temperature run with the updated mechanism
OLD-278K	low temperature run with CAABA/MECCA 4.5.5
High-NO_x	model run with the updated mechanism at high NO_x
Medium-NO_x	model run with the updated mechanism at medium NO_x
Low-NO_x	model run with the updated mechanism at low NO_x

Hodzic et al. (2014). For evaluating the impact of the new mechanism on ~~VOC~~ VOCs in different molecular size ranges, the total ~~LVOC~~ LVOCs has been subdivided into three groups: small-LVOC (up to four carbons), medium-LVOC (five and six carbons) and large-LVOC (more than six carbons). The new mechanism has a marginal impact on the simulated small-LVOC. Hence, this class is not included in the following discussion. Figure 6 shows mixing ratios of the BASE and the OLD sensitivity run at 298 K and 278 K, respectively. Mixing ratios of key radicals during all sensitivity runs are depicted in the supplement (see Fig. S10-S14).

The medium-LVOC displays the largest impact. Before sunrise (prior 8 h), no substantial mixing ratios are depicted. After sunrise, mixing ratios increase for the BASE and the OLD run, while the BASE run displays an approximately eight times higher peak mixing ratio. This is mainly due to the formation of MeBuTETROL and organosulfates from isoprene as shown in Fig. 7. The temperature change to 278 K lowers the medium-LVOC yield for both sensitivity runs, while the ratio between both remains similar. For the BASE run, the concentration decrease with temperature can be explained by a decrease in IEPOX formation in the ~~gas phase~~gas-phase, due to slower gas-phase oxidation rates (see OH mixing ratios in Fig. S13), with a simultaneous decrease of the acidity in the aqueous-phase (see Fig. S15). With the main SOA pathway of IEPOX being the acid-catalyzed ring-opening, a lower LVOC yield is expected. Nevertheless, the ratio of IEPOX between aqueous- and gas-phase increases, due to a higher partitioning coefficient ~~. In the global model, an~~ at low temperatures. IEPOX products increase the aerosol yield regardless of the temperature conditions. An increased production of SOA precursors from isoprene oxidation ~~is expected (see Carlton et al. (2009))~~at low NOx conditions is expected in future global model simulations (Carlton et al., 2009; Liu et al., 2016).

Large-LVOC also increase during the full simulation period with the introduced update, however, a less pronounced change is predicted. Even though limonene and its oxidation pathways are newly introduced and show non-negligible LVOC yields, the exclusion of camphene, sabinene, and carene compensates partly for the additional ~~LVOC~~LVOCs. For all three, a mechanism similar to α-pinene had been assumed, due to structural similarities. The oxidation of these monoterpenes will be re-introduced as soon as new experimental/theoretical results are accessible, including a compelling mechanism for all individual compounds. Several mechanistic studies involving camphene have been published recently ~~(Li et al., 2022; Subramani et al., 2021; Afreh et al., 2021)~~ (Subramani et al., 2021; Afreh et al., 2021; Li et al., 2022). Only before sunrise, when oxidation by ozone ~~and NO3~~ is domi-

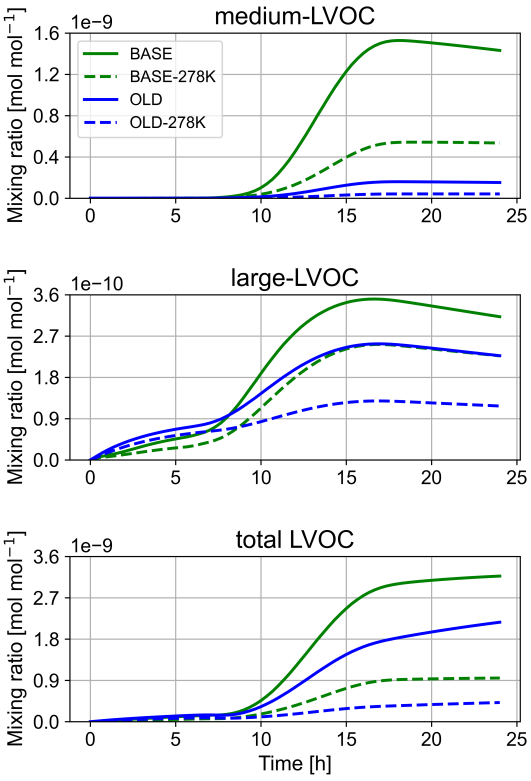

Figure 6. Temperature dependence of the ~~LVOC~~ LVOCs formation. Results from the BASE run are shown in green, while results from the OLD run are depicted in blue. The lower temperature runs BASE-278K and OLD-278K are displayed as dashed lines.

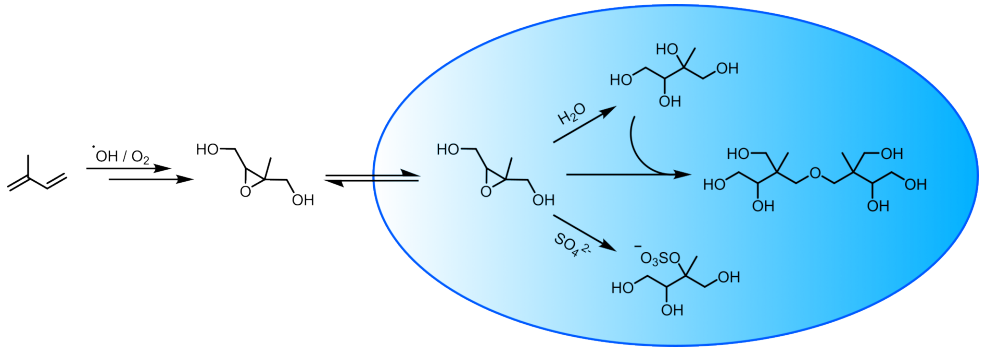

Figure 7. New aqueous-phase IEPOX scheme leading to the formation of polyols, organosulfates and oligomers.

nant, the OLD run out-competes the BASE run. This indicates a low LVOC yield in the limonene ozone mechanism for the chosen LVOC threshold. The total ~~LVOC~~ LVOCs show similar results as the medium-LVOC, together with a positive offset of both runs due to small-LVOC. Considering the reacted ~~VOC~~ VOCs and the produced ~~LVOC~~ LVOCs in the BASE run we can

calculate a LVOC yield to approximate the SOA yield. This analysis results in a yield of 7.3 %. With fixed isoprene concentration, it is the main LVOC contributor (approx. 90 %). Carlton et al. (2009) collected data from various studies investigating the SOA yield from isoprene and found yields up to 6 %. Taking into account that some loss processes are not implemented yet and that the aerosol formation process is not modeled, the agreement between model and experiment is reasonable.

3.2 ~~dependence~~

3.1.1 NO_x dependence

To estimate how anthropogenic NO_x emissions impact LVOC (and SOA) formation, we evaluate LVOC mixing ratios under varying NO_x concentrations. The main reactions of NO with peroxy radicals are O-abstraction and addition, forming alkoxy radicals and nitrates, respectively. These processes compete with the formation of hydroperoxides involving HO_2. As the products from NO oxidation are generally more volatile compared to hydroperoxides, less ~~LVOC~~ LVOCs are formed under high NO conditions. This hypothesis is supported by Pye et al. (2010), who estimated a low contribution of "RO_2 + NO"-reactions to the total aerosol fraction, while the "RO_2 + HO_2"-reaction shows a higher fraction for all considered compounds (biogenic ~~VOC~~VOCs). However, this ~~does not always hold true~~ is not always the case for aromatic compounds. Based on chamber studies, Xu et al. (2015a) found that the SOA yield and NO_x levels were correlated for toluene but anti-correlated for m-xylene. Figure 8 displays the model results of the sensitivity runs for the low-, medium-, and high-NO_x scenarios. NO initial mixing ratios were set to 20 pmol/mol for low, 2 nmol/mol for medium and 20 nmol/mol for modeling highly polluted areas. NO_2 mixing ratios are fixed to double the amount of NO mixing ratios. The large-LVOC ~~display~~ show the expected trend. With decreasing NO_x concentration, the mixing ratios increase as a result of the higher hydroperoxide product share. Especially large-LVOC formation before sunrise from ozone is strongly NO_x dependent. The medium-LVOC show a more complex behavior. LVOC mixing ratios rise between low and medium NO_x concentrations but fall off for high NO_x. This can be explained by the relative change of the OH concentration and the hydroperoxide yield. The OH concentration rises with increasing NO_x, while the hydroperoxide yield continuously decreases. IEPOX and many other LVOCs require the formation of an intermediate or product hydroperoxide group. At medium NO_x levels, the rise in ~~OH concentration overshadows~~ the OH concentration overwhelms the decreasing hydroperoxide yield for the dominant LVOC species. This trend reverses at high NO_x concentrations. Due to the comparably high total mixing ratios of the medium-LVOC bin, the total LVOC results reflect mainly the medium-LVOC.

3.2 ~~Aqueous-phase chemistry~~

3.1.1 Aqueous-phase chemistry

In the evaluation of the influence of temperature and NO_x on ~~LVOC~~LVOCs, the aqueous oxidation of IEPOX ~~displays~~ plays a key role and increases the complexity of the reaction system. Although the box model neglects many environmental effects and dependencies, we want to compare modeled with measured mixing ratios to see whether the model produces tracer com-

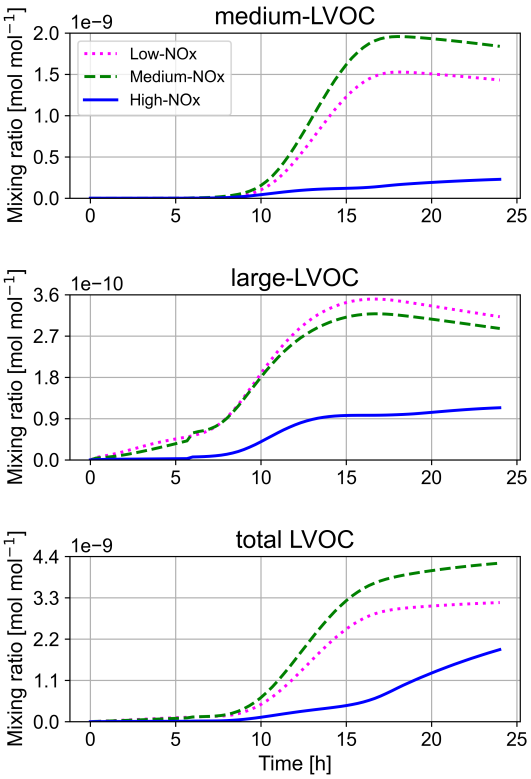

Figure 8. NO_x dependence of the LVOC formation. Results are displayed for low-NO_x (magenta, dotted line), medium-NO_x (green, dashed line) and high-NO_x (blue, solid line) NO_x mixing ratios. For definitions of low, medium and high, see text.

pounds in realistic amounts. For that reason, the model setup was adjusted to the conditions during the SOAS campaign (see Sect. 3.1.1). In this campaign, Hu et al. (2015) reported measurements of MeBuTETROL together with total IEPOX-SOA concentrations (combined concentrations of MeBuTETROL, C5-triols and isoprene-derived organic sulfates) in ambient aerosol. Assuming that the main IEPOX-SOA contributors are MeBuTETROL and the corresponding organosulfates (OS), the OS concentrations can be derived by subtracting the MeBuTETROL from the total IEPOX-SOA concentration. We extracted modeled concentrations after a full model day to compare the results. Note that this comparison is only intended to show whether the model yields results of the same order of magnitude. In measured mass concentrations, only MeBuTETROL found in aerosols is taken into account and general loss pathways are accessible (e.g. deposition). The model, on the other hand, adds up all products formed (gas- and aqueous-phase), and only the chemical loss of MeBuTETROL is considered. Wet and dry deposition and volatility based condensation are neglected in the model runs, which is expected to result in an over prediction of ~~LVOC~~LVOCs. Further, the modeled OH concentration exceeds the measurements (1.2~~E-13~~$\times 10^{-13}$ vs 5.5~~E-14~~$\times 10^{-14}$ $\mathrm{mol/mol}$, see Fig. S15 and Sanchez et al. (2018)), while the pH is higher in the model (Fig. S15) than in the SOAS aerosol (Guo et al. (2015), median pH of 1). The acid catalyzed ring-opening involving NO_3^- as nucleophile, described in Eddingsaas et al. (2010),

is also not considered. Thus, an over-prediction by the model is expected. Table 6 displays the mean measured and modeled MeBuTETROL, OS, and total IEPOX-SOA concentrations, with and without aqueous-phase degradation of MeBuTETROL. Modeled mass concentrations exceed the measured concentrations by an order of magnitude, while the MeBuTETROL over-prediction is 50 % higher without aqueous degradation (see Fig. 1). Considering the influence factors discussed above, this assessment lends confidence that the model for IEPOX-SOA is realistic. But it also stresses the importance of aqueous-phase degradation pathways in models. Non-negligible loss processes are still missing in the MECCA chemical scheme. The aqueous processing of all hydroperoxides, alkyl nitrates, and -sulfates is not implemented, resulting in an overestimation of those species. Additionally, there is no SAR method dealing with the reactivity of epoxides towards OH radicals in aqueous media. Reaction rates have to be estimated by treating epoxides like hydroxyl groups, not considering the enthalpy gained by prompt ~~ring opening~~ring-opening. On the other hand, organic coatings on aqueous aerosols and the aerosol phase state may limit the reactive uptake of IEPOX and thus the production of MeBuTETROL and OS (Zhang et al., 2018; Octaviani et al., 2021).

Table 6. Comparison between measured and modeled MeBuTETROL, OS and total IEPOX-SOA mass concentrations. Measured values are taken from Hu et al. (2015). The concentrations were investigated over multiple days, but a mean concentration of 0.3 $\frac{\mu g}{m^3}$ is assumed in the scope of this comparison. Modeled mixing ratios are extracted after a full modeled day.

Compound	**Measured / $\frac{\mu g}{m^3}$**	**Modeled / $\frac{\mu g}{m^3}$**	**Modeled no MeBuTETROL degrad. / $\frac{\mu g}{m^3}$**
	Hu et al. (2015)	**This work**	
MeBuTETROL	0.3	4.4	6.6
OS	0.6	5.3	4.4
total IEPOX-SOA	0.9	9.7	11.0

In addition to the LVOC concentrations, a change in the O/C ratio might occur as a result of the chemistry update. Especially, because ~~LVOC~~ LVOCs from aqueous oxidation is added, which commonly possesses a higher O/C ratio (Lim et al., 2010). The main LVOC components, MeBuTETROL and OS, exhibit a ratio of 1.0 and 1.6, respectively. Thus, an increase in the O/C ratio is expected. Figure 9 displays the O/C ratio of the aqueous ~~LVOC~~ LVOCs for the BASE and OLD run over the simulation time. After a full modeled day, an increase of 40 % is found, with a ratio of 0.98 and 0.70, for BASE and OLD, respectively. The updated model is in good agreement with the SOAS campaign average O/C ratio of 0.91 (Massoli et al., 2018). More accurate degradation pathways of MeBuTETROL and OS are expected to further improve the O/C ratio.

In addition to the already described aqSOA formation sources, there are further known, but missing processes not covered by the mechanism. Formation of nitroaromatics from the aqueous-phase oxidation of anthropogenic ~~VOC~~ VOCs is an important additional source of aqSOA. For instance, it has been shown that 4 % to 20 % of total SOA in Europe is aqSOA originating from residential wood burning (Gilardoni et al., 2016). Accounting for this source of aqSOA requires the development of an explicit mechanism for heterogeneous reactions of N_2O_5 where chloride and phenols compete with water for the addition to NO_2^+ (Heal et al., 2007; Ryder et al., 2015; Hoffmann et al., 2018; Staudt et al., 2019). A simplified scheme for the nitration of phenol has recently been implemented into MECCA by Soni et al. (2023). Moreover, consideration of nitroaromatics during

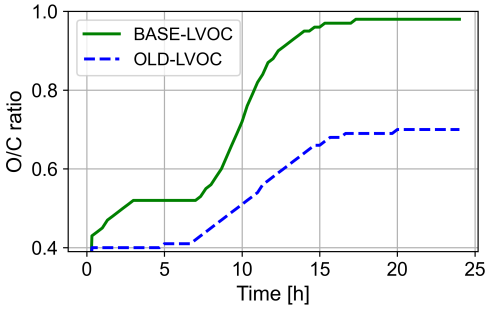

Figure 9. O/C ratio of summed up ~~LVOC~~ LVOCs for the BASE and OLD run.

nighttime oxidation of furans from biomass burning will further increase the model predictions of SOA mass (Joo et al., 2019; Al Ali et al., 2022).

3.2 Model-chamber comparison

3.2.1 Experimental setup and considerations

Model results are compared to data from two experiments carried out in the SAPHIR (Simulation of Atmospheric PHotochemistry in a large Reaction chamber) chamber for further validation of the chemical mechanism. More information about the SAPHIR chamber can be found elsewhere (Rohrer et al., 2005; Karl et al., 2006; Schlosser et al., 2007). The newly implemented limonene mechanism is tested by simulating an experiment on the ozonolysis of limonene in the dark with subsequent aerosol aging by NO_3 (Gkatzelis et al., 2018). Thereby, the performance of the modified MCM scheme is assessed (see Sect. 2.3.2). The potential impact of the new mechanism on SOA is investigated by looking into the organic mass and the aerosol O/C ratio. The O/C ratio measured by an aerosol mass spectrometer (AMS) is used in an already corrected form, as presented in Canagaratna et al. (2015). The full isoprene-NO3 mechanism by Vereecken et al. (2021) was previously compared to results of chamber experiments in SAPHIR (Vereecken et al., 2021). Since the mechanism included in this work is a subset of this scheme, we decided to compare it with the same chamber experiment to investigate, whether using the subset gives similar results. Thus, we focus on gas-phase reactions and products. Alkyl nitrate (AN) and peroxy radical (RO_2) concentrations from model simulations based on the old and new isoprene-NO_3 mechanisms were compared to each other. RO_2 concentrations are additionally compared to measured data. For RO_2 measurements, some adjustments were applied to the model results. RO_2 radicals are not directly measured by the laser-induced fluorescence (LIF) instrument used in the campaign. To detect RO_2, they are first converted to alkoxy radicals in the reaction with NO. Formed alkoxy radicals are then expected to undergo H-abstration by O_2 yielding HO_2, which is measured by the LIF (Fuchs et al., 2008). Thus, measurement results depend on the HO_2-yield from the given alkoxy radical. For some alkoxy radicals like the methyl alkoxy radical, this yield is close to 100 % (Novelli et al., 2021; Vereecken et al., 2021). However, Novelli et al. (2021) investigated competitive reaction pathways for alkoxy radicals containing a nitrate group. In some cases, they found that decomposition (NO_2-elimination)

and isomerization reactions can compete with the HO_2 production. This complicates model-experiment comparisons. To fit model results better to the RO_2 detectable by the LIF instrument, Vereecken et al. derived the subset for individual Isoprene-NO_3 products that yields HO_2 (see SI of Vereecken et al. (2021)). Similar to Vereecken et al. (2021) we use these values to calculate the detectable RO_2 from the total RO_2. In contrast to the mechanism by Vereecken et al. not all compounds with stereochemistry are included with all isomers in the subset scheme, but are treated as lumped species. For those species, the correction for detectability is done as if the lumped species consist of 50 % of each isomer. Due to the strong dependency of the results on the NO_3 and HO_2 concentrations, model concentrations were constrained to measured data. Isoprene injections were adjusted to reproduce the observed increase in the concentration measurements of the VOCUS instrument (see Brownwood et al. (2021)). VOCUS data were corrected by a factor of 0.7 to account for the measurement's dependency on water.

Chamber injections were modeled as the increase of the injected chemical to the measured peak values within one timestep. In Table 7 all injections are listed. For the limonene and isoprene experiment dilution effects are modeled using a rate of $4.8\%h^{-1}$ and $5.6\%h^{-1}$, respectively. Dilution rates are calculated from the mean total flow during the experiments. For the limonene experiment, this rate is applied to gas and aerosol species. The high volume-to-surface ratio of the SAPHIR chamber minimizes the wall losses and are not considered as a first approximation. Especially, particle wall loss is discussed in Sect. 3.2.2. The aerosol liquid water content (ALWC) is estimated based on AMS measurements of the high resolution H_2O signal, which represents an approximate upper limit. This signal is influenced by interference of organics. Further information about the experiments is shown in Section 5 of the SI.

Table 7. Injections used in modeling of the chamber experiments. Model injections refer to an instantaneous change of the given mixing ratio after the previous timestep.

Limonene + Ozone				
Injection No.	**Limonene [ppb]**	**Ozone [ppb]**	**NO [ppb]**	**time since start [min]**
1	23.6	140	-	0
2	-	-	30	450
Isoprene + NO_3				
Injection No.	**Isoprene [ppb]**	**Ozone [ppb]**	**NO_2 [ppb]**	**time since start [min]**
1	-	105	24	0
2	5.1	-	-	5
3	8.0	108	23	117
4	7.0	102	25	202
5	-	111	23	360

3.2.2 Limonene + Ozone

The modeled and measured organic mass concentration (OM) is displayed in Fig. 10. Both modeled and measured mass concentrations increase rapidly at the start of the experiment. The experimental OM decreases after one hour, while the model still predicts an increase. This is due to missing loss processes in the model as only the dilution of gas- and aerosol-phase species is considered, although species are also lost to the chamber walls. Schmitt (2018) has shown, that particle losses to chamber walls in the SAPHIR chamber can be higher than the dilution. Figure S18 shows results for the organic mass with simplified aerosol wall loss, with a loss rate similar to Schmitt (2018). This test simulation indicates, that a larger portion of the over-prediction is due to missing particle loss. The nucleation and condensation of pure organics is also not modeled (see Sect. 2.2). Additionally, in the model, large compounds (> C_4) in the aerosol phase are currently not further oxidized (except isoprene and methylglyoxal products) (Rosanka et al., 2021), resulting in an insufficient chemical loss of organics. This missing oxidation is also reflected in the aerosol O/C ratio. In the experiment, the measured O/C ratio is in the range between 0.56-0.66, while the model predicts values between 0.4-0.51 with a similar trend (see Fig. S16). The nitrogen oxide injection after 7.5 h leads to an OM increase in both simulation and experiment. As a result of the overall higher OM and thus in total more oxidizable compounds, the model results show a steeper OM increase after the NO injection.

The experimental data was modeled without constraining the radical concentrations to experimental values. OM and O/C

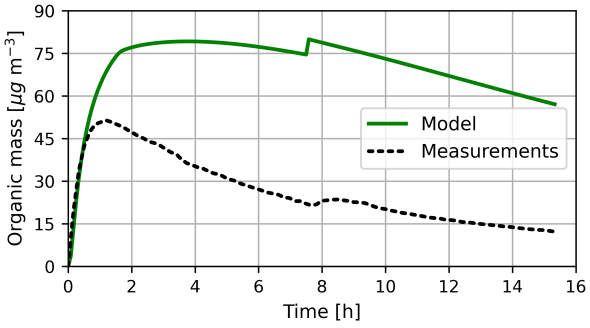

Figure 10. Mass concentration of OM in model and experiment. Modeled OM represents all species with an H_s of larger than 4×10^6 M/atm in either gas- or aqueous-phase. This simplification is applied to account for missing processes in the model. After 7.5 h NO is injected into the chamber.

ratio values are strongly connected to the amount of limonene consumed by the different radicals (OH, ozone). As the OH concentration were not measured, the modeled OH concentration cannot be validated with experimental results. Thus, model results might be affected by incorrect radical concentrations. Figure S17 displays the OH reactivity in the model and the experiment, implying an underestimation of OH in the model.

3.2.3 Isoprene + NO_3

The modeled and measured organic peroxide radical (RO_2) mixing ratios are displayed in Fig. 11. As the new isoprene-NO_3 mechanism is an update to the previously used mechanism (in contrast to limonene), experimental results are compared to the

old and new mechanism representations. The detectable RO_2 is only determined for the new mechanism, as the HO_2-yields are unknown for the RO_2 formed in the old scheme (see Sect 3.2.1).

All model simulations over-predict RO_2 concentrations, especially shortly after the VOC injections. Measured RO_2 level trends after the initial peaks show reasonable agreement between the experiment and detectable RO_2 of the new mechanism. Especially during times, when the RO_2 concentration decreases, the detectable RO_2 is in good agreement with the experimental results. The old mechanism shows an offset during times when the RO_2 concentration decreases, indicating the formation of a sufficiently stable RO_2. The RO_2 results are comparable to the simulation by Vereecken et al. (2021). Simulation results are influenced by how model variables are constrained to measured data. In Vereecken et al. (2021) constrained radical levels are fitted to experimental data, while in CAABA/MECCA concentrations are set to the exact value measured. Thus, radical (HO_2 and NO_3) concentrations in Vereecken et al. (2021) are higher, close to the injection than in the present study.

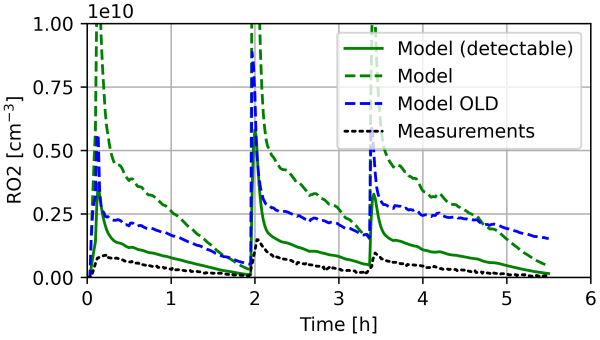

Figure 11. RO_2 mixing ratios in model and experiment. Model results marked with "detectable" are modified by HO_x formation efficiencies by Vereecken et al. (2021).

Figure 12 displays the AN mixing ratio as a function of isoprene consumed by NO_3 calculated by rate constants and concentrations from the model. Mixing ratios predicted by the new mechanism are 10-20% lower than results from the old scheme. Although a higher variety of AN products are accessible, in the new scheme, also more loss processes are considered. Especially compounds, that are only lost to OH radicals in the old mechanism, like 1-Hydroxy-2-propanone nitrate (NOA), keep the AN concentration at high levels in the old run. Throughout the isoprene-NO_3 campaign, an average of 108 $\pm$ 15 % of ANs was derived which is in reasonable agreement with the model simulations with the new mechanism (84-93 % AN yield). AN yields of the old mechanism are even closer to the measurements (98-116% AN yield). The slight under-prediction of the new model is likely due to the decomposition of organic nitrates forming small oxidized compounds and NO_2 in the degradation process. The faster AN loss processes are a potential artifact of the missing reactions from the original scheme. Nevertheless, various products in the new scheme are expected to increase the modeled SOA yield in future global simulations. Among them are functionalized epoxides and hydroperoxy nitrates.

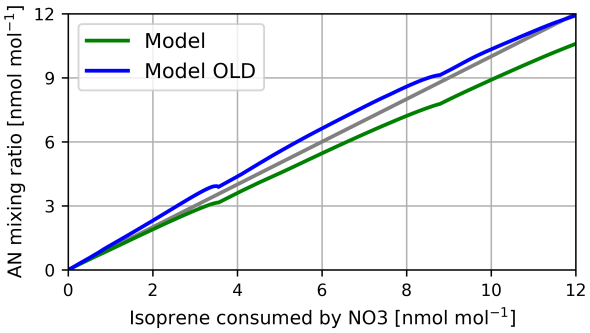

Figure 12. AN mixing ratios against isoprene consumed by NO_3. The gray line displays the one-to-one line.

4 Summary and Outlook

~~The chemical scheme of MECCA has been updated~~

We updated the chemical scheme of MECCA to improve the production of SOA precursors in the model. In addition, we investigated the gas-/aqueous-phase partitioning of the new species formed. To assess the update, we investigated the production of ~~LVOC~~ LVOCs at different physical conditions and initial concentrations in a box model. As expected, we find an increase in the total mixing ratio of ~~LVOC, while~~ LVOCs and also the change in ~~LVOC~~ LVOCs of different sizes is more pronounced. Results display a rising production of medium- and large-sized ~~LVOC~~LVOCs, while the number of small ~~LVOC~~ LVOCs stays constant. This is due to the new implementation of exclusively medium to large precursors. By changing the temperature from 298 K to 278 K, the model predicts a decrease in LVOC production, while an increase in SOA yield is expected. This can be attributed to the simplified way SOA is accounted for. The NO_x-dependence shows more complex patterns of change. In general, the LVOC yield decreases with rising NO_x, but for medium-LVOC, an increase at moderate NO_x is found. This is due to the aqueous-phase IEPOX oxidation scheme. The modeled O/C ratio confirms the ~~experimental results~~ aerosol measurements of the SOAS campaign. Model simulations of chamber experiments generally aligned with experimental results, especially considering the model limitations influencing the limonene-ozone experiment. Overall, we find that the model responds differently to newly added aqueous- and gas-phase reactions. ~~To~~ Gas-phase processes are well modeled by the new mechanism. To also better reflect the processing of ~~VOC and LVOC~~ VOCs and LVOCs in clouds and aerosols, more aqueous-phase reactions, also for the small and large compounds are needed. Furthermore, the implementation of recent findings concerning the peroxy radical reactivity might lead to additional reaction pathways or altered branching ratios Schervish and Donahue (2021); Mayorga et al. (2022). H-shifts of peroxy radicals are only considered in the new limonene mechanism and might lead to an increased formation of HOMs in the model if included for all compounds (Wu et al., 2021). Similarly, the treatment of peroxy radical dimerization was found to be more important than previously estimated (Schervish and Donahue, 2020). In future work, we ~~want to~~ will evaluate the impact of the new mechanism on SOA precursors with explicit multiphase kinetics in deliquescent aerosols and cloud droplets in the global model EMAC (Rosanka et al., 2023). To investigate the dependence of results on the partitioning scheme and the used Henry's law solubility constants at the global scale, sensitivity runs will be executed with varying partitioning scheme. Further, the introduction of more SOA/LVOC loss processes to the model has shown to be important, as already pointed out by Hodzic et al. (2016). A general aqueous-phase degradation scheme of organic nitrates and hydroperoxides would further refine SOA processes.

Code availability. The updated MECCA model code is available as a community model published under the GNU General Public License (https://www.gnu.org/copyleft/gpl.html). The model code can be found in the Supplement (DOI:10.5281/zenodo.7944174) and in the code repository at https://gitlab.com/RolfSander/caaba-mecca. In addition to the complete code, a list of chemical reactions including rate constants and references (meccanism.pdf) and a user manual (caaba_mecca_manual.pdf) are available in the manual directory of the supplement. A list of all Henry's law and accommodation constants (chemprop.pdf) is available in the tools/chemprop directory. For further information and updates, the CAABA/MECCA web page at http://www.mecca.messy-interface.org can be consulted.

Author contributions. FW and DT designed the study and developed the chemical mechanism. The latter was reviewed by all co-authors and implemented into MECCA by FW and RS. FW performed the estimation of the Henry's law coefficients. The manuscript was prepared by FW and reviewed by all co-authors. The measurements were carried out and analyzed by CC, AN, HF, RT and TH.

Competing interests. Some authors are members of the editorial board of GMD. The peer-review process was guided by an independent editor, and the authors have also no other competing interests to declare.

Acknowledgements. The authors gratefully acknowledge the computing time granted through JARA on the supercomputer JURECA (Jülich Supercomputing Centre, 2021) at Forschungszentrum Jülich.

References

Afreh, I. K., Aumont, B., Camredon, M., and Barsanti, K. C.: Using GECKO-A to derive mechanistic understanding of secondary organic aerosol formation from the ubiquitous but understudied camphene, Atmospheric Chemistry and Physics, 21, 11 467–11 487, 2021.

Al Ali, F., Coeur, C., Houzel, N., Bouya, H., Tomas, A., and Romanias, M. N.: Rate Coefficients for the Gas-Phase Reactions of Nitrate Radicals with a Series of Furan Compounds, The Journal of Physical Chemistry A, 126, 8674–8681, https://doi.org/10.1021/acs.jpca.2c03828, publisher: American Chemical Society, 2022.

Arey, J., Aschmann, S. M., Kwok, E. S. C., and Atkinson, R.: Alkyl Nitrate, Hydroxyalkyl Nitrate, and Hydroxycarbonyl Formation from the NOx-Air Photooxidations of C5-C8 n-Alkanes, The Journal of Physical Chemistry A, 105, 1020–1027, https://doi.org/10.1021/jp003292z, publisher: American Chemical Society, 2001.

Atkinson, R., Arey, J., and Aschmann, S. M.: Atmospheric chemistry of alkanes: Review and recent developments, Atmospheric Environment, 42, 5859–5871, https://doi.org/10.1016/j.atmosenv.2007.08.040, 2008.

Ayres, B., Allen, H., Draper, D., Brown, S., Wild, R., Jimenez, J., Day, D., Campuzano-Jost, P., Hu, W. d., De Gouw, J., et al.: Organic nitrate aerosol formation via NO 3+ biogenic volatile organic compounds in the southeastern United States, Atmospheric Chemistry and Physics, 15, 13 377–13 392, 2015.

Bates, K. H., Crounse, J. D., St. Clair, J. M., Bennett, N. B., Nguyen, T. B., Seinfeld, J. H., Stoltz, B. M., and Wennberg, P. O.: Gas phase production and loss of isoprene epoxydiols, The Journal of Physical Chemistry A, 118, 1237–1246, https://doi.org/10.1021/jp4107958, 2014.

Brownwood, B., Turdziladze, A., Hohaus, T., Wu, R., Mentel, T. F., Carlsson, P. T., Tsiligiannis, E., Hallquist, M., Andres, S., Hantschke, L., et al.: Gas-particle partitioning and SOA yields of organonitrate products from NO3-initiated oxidation of isoprene under varied chemical regimes, ACS earth and space chemistry, 5, 785–800, 2021.

Budisulistiorini, S., Li, X., Bairai, S., Renfro, J., Liu, Y., Liu, Y., McKinney, K., Martin, S., McNeill, V., Pye, H., et al.: Examining the effects of anthropogenic emissions on isoprene-derived secondary organic aerosol formation during the 2013 Southern Oxidant and Aerosol Study (SOAS) at the Look Rock, Tennessee ground site, Atmospheric Chemistry and Physics, 15, 8871–8888, 2015.

Cabrera-Perez, D., Taraborrelli, D., Sander, R., and Pozzer, A.: Global atmospheric budget of simple monocyclic aromatic compounds, Atmospheric Chemistry and Physics, 16, 6931–6947, https://doi.org/10.5194/acp-16-6931-2016, 2016.

Canagaratna, M., Jimenez, J., Kroll, J., Chen, Q., Kessler, S., Massoli, P., Hildebrandt Ruiz, L., Fortner, E., Williams, L., Wilson, K., et al.: Elemental ratio measurements of organic compounds using aerosol mass spectrometry: characterization, improved calibration, and implications, Atmospheric Chemistry and Physics, 15, 253–272, 2015.

Carlsson, P. T. M., Vereecken, L., Novelli, A., Bernard, F., Brown, S. S., Brownwood, B., Cho, C., Crowley, J. N., Dewald, P., Edwards, P. M., Friedrich, N., Fry, J. L., Hallquist, M., Hantschke, L., Hohaus, T., Kang, S., Liebmann, J., Mayhew, A. W., Mentel, T., Reimer, D., Rohrer, F., Shenolikar, J., Tillmann, R., Tsiligiannis, E., Wu, R., Wahner, A., Kiendler-Scharr, A., and Fuchs, H.: Comparison of isoprene chemical mechanisms under atmospheric night-time conditions in chamber experiments: evidence of hydroperoxy aldehydes and epoxy products from NO_3 oxidation, Atmospheric Chemistry and Physics, 23, 3147–3180, https://doi.org/10.5194/acp-23-3147-2023, publisher: Copernicus GmbH, 2023.

Carlton, A., Wiedinmyer, C., and Kroll, J.: A review of Secondary Organic Aerosol (SOA) formation from isoprene, Atmospheric Chemistry and Physics, 9, 4987–5005, https://doi.org/10.5194/acp-9-4987-2009, 2009.

Carlton, A. G., Turpin, B. J., Altieri, K. E., Seitzinger, S., Reff, A., Lim, H.-J., and Ervens, B.: Atmospheric oxalic acid and SOA production from glyoxal: Results of aqueous photooxidation experiments, Atmospheric Environment, 41, 7588–7602, https://doi.org/10.1016/j.atmosenv.2007.05.035, 2007.

Carslaw, N.: A mechanistic study of limonene oxidation products and pathways following cleaning activities, Atmospheric Environment, 80, 507–513, https://doi.org/10.1016/j.atmosenv.2013.08.034, 2013.

Chen, D., Zhao, Y., Zhang, J., Yu, H., and Yu, X.: Characterization and source apportionment of aerosol light scattering in a typical polluted city in the Yangtze River Delta, China, Atmospheric Chemistry and Physics, 20, 10 193–10 210, https://doi.org/10.5194/acp-20-10193-2020, 2020.

Cope, J. D., Abellar, K. A., Bates, K. H., Fu, X., and Nguyen, T. B.: Aqueous photochemistry of 2-Methyltetrol and erythritol as sources of formic acid and acetic acid in the atmosphere, ACS Earth and Space Chemistry, 5, 1265–1277, https://doi.org/10.1021/acsearthspacechem.1c00107, 2021.

D'Ambro, E. L., Møller, K. H., Lopez-Hilfiker, F. D., Schobesberger, S., Liu, J., Shilling, J. E., Lee, B. H., Kjaergaard, H. G., and Thornton, J. A.: Isomerization of second-generation isoprene peroxy radicals: Epoxide formation and implications for secondary organic aerosol yields, Environmental science & technology, 51, 4978–4987, https://doi.org/10.1021/acs.est.7b00460, 2017.

Eddingsaas, N. C., VanderVelde, D. G., and Wennberg, P. O.: Kinetics and products of the acid-catalyzed ring-opening of atmospherically relevant butyl epoxy alcohols, The Journal of Physical Chemistry A, 114, 8106–8113, 2010.

Ehrhart, S., Dunne, E. M., Manninen, H. E., Nieminen, T., Lelieveld, J., and Pozzer, A.: Two new submodels for the Modular Earth Submodel System (MESSy): New Aerosol Nucleation (NAN) and small ions (IONS) version 1.0, Geoscientific Model Development, 11, 4987–5001, 2018.

Ervens, B.: Modeling the processing of aerosol and trace gases in clouds and fogs, Chemical reviews, 115, 4157–4198, https://doi.org/10.1021/cr5005887, 2015.

Franco, B., Blumenstock, T., Cho, C., Clarisse, L., Clerbaux, C., Coheur, P.-F., De Mazière, M., De Smedt, I., Dorn, H.-P., Emmerichs, T., Fuchs, H., Gkatzelis, G., Griffith, D. W. T., Gromov, S., Hannigan, J. W., Hase, F., Hohaus, T., Jones, N., Kerkweg, A., Kiendler-Scharr, A., Lutsch, E., Mahieu, E., Novelli, A., Ortega, I., Paton-Walsh, C., Pommier, M., Pozzer, A., Reimer, D., Rosanka, S., Sander, R., Schneider, M., Strong, K., Tillmann, R., Van Roozendael, M., Vereecken, L., Vigouroux, C., Wahner, A., and Taraborrelli, D.: Ubiquitous atmospheric production of organic acids mediated by cloud droplets, Nature, 593, 233–237, https://doi.org/10.1038/s41586-021-03462-x, number: 7858 Publisher: Nature Publishing Group, 2021.

Fuchs, H., Holland, F., and Hofzumahaus, A.: Measurement of tropospheric RO2 and HO2 radicals by a laser-induced fluorescence instrument, Review of Scientific Instruments, 79, 2008.

Gilardoni, S., Massoli, P., Paglione, M., Giulianelli, L., Carbone, C., Rinaldi, M., Decesari, S., Sandrini, S., Costabile, F., Gobbi, G. P., et al.: Direct observation of aqueous secondary organic aerosol from biomass-burning emissions, Proceedings of the National Academy of Sciences, 113, 10 013–10 018, 2016.

Gkatzelis, G. I., Tillmann, R., Hohaus, T., Müller, M., Eichler, P., Xu, K.-M., Schlag, P., Schmitt, S. H., Wegener, R., Kaminski, M., et al.: Comparison of three aerosol chemical characterization techniques utilizing PTR-ToF-MS: a study on freshly formed and aged biogenic SOA, Atmospheric Measurement Techniques, 11, 1481–1500, 2018.

Guo, H., Xu, L., Bougiatioti, A., Cerully, K. M., Capps, S. L., Hite Jr, J., Carlton, A., Lee, S.-H., Bergin, M., Ng, N., et al.: Fine-particle water and pH in the southeastern United States, Atmospheric Chemistry and Physics, 15, 5211–5228, 2015.

Hallquist, M., Wenger, J. C., Baltensperger, U., Rudich, Y., Simpson, D., Claeys, M., Dommen, J., Donahue, N., George, C., Goldstein, A., et al.: The formation, properties and impact of secondary organic aerosol: current and emerging issues, Atmospheric chemistry and physics, 9, 5155–5236, https://doi.org/10.5194/acp-9-5155-2009, 2009.

Heal, M. R., Harrison, M. A. J., and Neil Cape, J.: Aqueous-phase nitration of phenol by N2O5 and ClNO2, Atmospheric Environment, 41, 3515–3520, https://doi.org/10.1016/j.atmosenv.2007.02.003, 2007.

Heald, C., Coe, H., Jimenez, J., Weber, R., Bahreini, R., Middlebrook, A., Russell, L., Jolleys, M., Fu, T.-M., Allan, J., et al.: Exploring the vertical profile of atmospheric organic aerosol: comparing 17 aircraft field campaigns with a global model, Atmospheric Chemistry and Physics, 11, 12 673–12 696, https://doi.org/10.5194/acp-11-12673-2011, 2011.

Hens, K., Novelli, A., Martinez, M., Auld, J., Axinte, R., Bohn, B., Fischer, H., Keronen, P., Kubistin, D., Nölscher, A. C., Oswald, R., Paasonen, P., Petäjä, T., Regelin, E., Sander, R., Sinha, V., Sipilä, M., Taraborrelli, D., Tatum Ernest, C., Williams, J., Lelieveld, J., and Harder, H.: Observation and modelling of HO_x radicals in a boreal forest, Atmospheric Chemistry and Physics, 14, 8723–8747, https://doi.org/10.5194/acp-14-8723-2014, publisher: Copernicus GmbH, 2014.

Herrmann, H., Schaefer, T., Tilgner, A., Styler, S. A., Weller, C., Teich, M., and Otto, T.: Tropospheric aqueous-phase chemistry: kinetics, mechanisms, and its coupling to a changing gas phase, Chemical reviews, 115, 4259–4334, 2015.

Hodzic, A., Aumont, B., Knote, C., Lee-Taylor, J., Madronich, S., and Tyndall, G.: Volatility dependence of Henry's law constants of condensable organics: Application to estimate depositional loss of secondary organic aerosols, Geophysical Research Letters, 41, 4795–4804, https://doi.org/10.1002/2014GL060649, 2014.

Hodzic, A., Kasibhatla, P. S., Jo, D. S., Cappa, C. D., Jimenez, J. L., Madronich, S., and Park, R. J.: Rethinking the global secondary organic aerosol (SOA) budget: stronger production, faster removal, shorter lifetime, Atmospheric Chemistry and Physics, 16, 7917–7941, https://doi.org/10.5194/acp-16-7917-2016, 2016.

Hoffmann, Erik, H., Tilgner, A., Wolke, R., Böge, O., Walter, A., and Herrmann, H.: Oxidation of substituted aromatic hydrocarbons in the tropospheric aqueous phase: kinetic mechanism development and modelling, Physical Chemistry Chemical Physics, 20, 10 960–10 977, https://doi.org/10.1039/C7CP08576A, publisher: Royal Society of Chemistry, 2018.

Hu, W., Campuzano-Jost, P., Palm, B., Day, D., Ortega, A., Hayes, P., Krechmer, J., Chen, Q., Kuwata, M., Liu, Y., et al.: Characterization of a real-time tracer for isoprene epoxydiols-derived secondary organic aerosol (IEPOX-SOA) from aerosol mass spectrometer measurements, Atmospheric Chemistry and Physics, 15, 11 807–11 833, https://doi.org/10.5194/acp-15-11807-2015, 2015.

Jenkin, M., Saunders, S. M., and Pilling, M. J.: The tropospheric degradation of volatile organic compounds: A protocol for mechanism development, Atmos. Environ., 31, 81–104, https://doi.org/10.1016/S1352-2310(96)00105-7, 1997.

Jöckel, P., Tost, H., Pozzer, A., Brühl, C., Buchholz, J., Ganzeveld, L., Hoor, P., Kerkweg, A., Lawrence, M., Sander, R., et al.: The atmospheric chemistry general circulation model ECHAM5/MESSy1: consistent simulation of ozone from the surface to the mesosphere, Atmospheric Chemistry and Physics, 6, 5067–5104, 2006.

Jöckel, P., Kerkweg, A., Pozzer, A., Sander, R., Tost, H., Riede, H., Baumgaertner, A., Gromov, S., and Kern, B.: Development cycle 2 of the modular earth submodel system (MESSy2), Geoscientific Model Development, 3, 717–752, https://doi.org/10.5194/gmd-3-717-2010, 2010.

Jöckel, P., Tost, H., Pozzer, A., Kunze, M., Kirner, O., Brenninkmeijer, C. A., Brinkop, S., Cai, D. S., Dyroff, C., Eckstein, J., et al.: Earth system chemistry integrated modelling (ESCiMo) with the modular earth submodel system (MESSy) version 2.51, Geoscientific Model Development, 9, 1153–1200, 2016.

Joo, T., Rivera-Rios, J. C., Takeuchi, M., Alvarado, M. J., and Ng, N. L.: Secondary Organic Aerosol Formation from Reaction of 3-Methylfuran with Nitrate Radicals, ACS Earth and Space Chemistry, 3, 922–934, https://doi.org/10.1021/acsearthspacechem.9b00068, publisher: American Chemical Society, 2019.

Jülich Supercomputing Centre: JURECA: Data Centric and Booster Modules implementing the Modular Supercomputing Architecture at Jülich Supercomputing Centre, Journal of large-scale research facilities, 7, https://doi.org/10.17815/jlsrf-7-182, 2021.

Kampf, C. J., Waxman, E. M., Slowik, J. G., Dommen, J., Pfaffenberger, L., Praplan, A. P., Prévôt, A. S., Baltensperger, U., Hoffmann, T., and Volkamer, R.: Effective Henry's law partitioning and the salting constant of glyoxal in aerosols containing sulfate, Environmental science & technology, 47, 4236–4244, 2013.

Karl, M., Dorn, H.-P., Holland, F., Koppmann, R., Poppe, D., Rupp, L., Schaub, A., and Wahner, A.: Product study of the reaction of OH radicals with isoprene in the atmosphere simulation chamber SAPHIR, Journal of atmospheric chemistry, 55, 167–187, 2006.

Kerkweg, A., Sander, R., Tost, H., Jöckel, P., and Lelieveld, J.: Simulation of detailed aerosol chemistry on the global scale using MECCA-AERO, Atmospheric Chemistry and Physics, 7, 2973–2985, 2007.

Kühne, R., Ebert, R.-U., and Schüürmann, G.: Prediction of the temperature dependency of Henry's law constant from chemical structure, Environmental science & technology, 39, 6705–6711, https://doi.org/10.1021/es050527h, 2005.

Kwok, E. S. and Atkinson, R.: Estimation of hydroxyl radical reaction rate constants for gas-phase organic compounds using a structure-reactivity relationship: An update, Atmospheric Environment, 29, 1685–1695, 1995.

Li, Q., Jiang, J., Afreh, I. K., Barsanti, K. C., and Cocker III, D. R.: Secondary organic aerosol formation from camphene oxidation: measurements and modeling, Atmospheric Chemistry and Physics, 22, 3131–3147, 2022.

Lim, Y., Tan, Y., Perri, M., Seitzinger, S., and Turpin, B.: Aqueous chemistry and its role in secondary organic aerosol (SOA) formation, Atmospheric Chemistry and Physics, 10, 10 521–10 539, https://doi.org/10.5194/acp-10-10521-2010, 2010.

Lin, G., Sillman, S., Penner, J., and Ito, A.: Global modeling of SOA: the use of different mechanisms for aqueous-phase formation, Atmospheric Chemistry and Physics, 14, 5451–5475, https://doi.org/10.5194/acp-14-5451-2014, 2014.

Lin, Y.-H., Arashiro, M., Clapp, P. W., Cui, T., Sexton, K. G., Vizuete, W., Gold, A., Jaspers, I., Fry, R. C., and Surratt, J. D.: Gene expression profiling in human lung cells exposed to isoprene-derived secondary organic aerosol, Environmental science & technology, 51, 8166–8175, https://doi.org/10.1021/acs.est.7b01967, 2017.

Liu, J., D'Ambro, E. L., Lee, B. H., Lopez-Hilfiker, F. D., Zaveri, R. A., Rivera-Rios, J. C., Keutsch, F. N., Iyer, S., Kurten, T., Zhang, Z., et al.: Efficient isoprene secondary organic aerosol formation from a non-IEPOX pathway, Environmental science & technology, 50, 9872–9880, 2016.

Lopez-Hilfiker, F., Mohr, C., D'ambro, E., Lutz, A., Riedel, T., Gaston, C., Iyer, S., Zhang, Z., Gold, A., Surratt, J., et al.: Molecular composition and volatility of organic aerosol in the Southeastern US: implications for IEPOX derived SOA, Environmental science & technology, 50, 2200–2209, https://doi.org/10.1021/acs.est.5b04769, 2016.

Mallik, C., Tomsche, L., Bourtsoukidis, E., Crowley, J. N., Derstroff, B., Fischer, H., Hafermann, S., Hüser, I., Javed, U., Keßel, S., Lelieveld, J., Martinez, M., Meusel, H., Novelli, A., Phillips, G. J., Pozzer, A., Reiffs, A., Sander, R., Taraborrelli, D., Sauvage, C., Schuladen, J., Su, H., Williams, J., and Harder, H.: Oxidation processes in the eastern Mediterranean atmosphere: evidence from the modelling of HO_x measurements over Cyprus, Atmospheric Chemistry and Physics, 18, 10 825–10 847, https://doi.org/10.5194/acp-18-10825-2018, publisher: Copernicus GmbH, 2018.

Massoli, P., Stark, H., Canagaratna, M. R., Krechmer, J. E., Xu, L., Ng, N. L., Mauldin III, R. L., Yan, C., Kimmel, J., Misztal, P. K., et al.: Ambient measurements of highly oxidized gas-phase molecules during the southern oxidant and aerosol study (SOAS) 2013, ACS Earth and Space Chemistry, 2, 653–672, 2018.

Mayorga, R., Xia, Y., Zhao, Z., Long, B., and Zhang, H.: Peroxy radical autoxidation and sequential oxidation in organic nitrate formation during limonene nighttime oxidation, Environmental Science & Technology, 56, 15 337–15 346, 2022.

McDonald, B. C., de Gouw, J. A., Gilman, J. B., Jathar, S. H., Akherati, A., Cappa, C. D., Jimenez, J. L., Lee-Taylor, J., Hayes, P. L., McKeen, S. A., Cui, Y. Y., Kim, S.-W., Gentner, D. R., Isaacman-VanWertz, G., Goldstein, A. H., Harley, R. A., Frost, G. J., Roberts, J. M., Ryerson, T. B., and Trainer, M.: Volatile chemical products emerging as largest petrochemical source of urban organic emissions, Science, 359, 760–764, https://doi.org/10.1126/science.aaq0524, publisher: American Association for the Advancement of Science, 2018.

Mekic, M. and Gligorovski, S.: Ionic strength effects on heterogeneous and multiphase chemistry: Clouds versus aerosol particles, Atmospheric Environment, 244, 117 911, 2021.

Meylan, W. M. and Howard, P. H.: Bond contribution method for estimating henry's law constants, Environmental Toxicology and Chemistry, 10, 1283–1293, https://doi.org/10.1002/etc.5620101007, _eprint: https://onlinelibrary.wiley.com/doi/pdf/10.1002/etc.5620101007, 1991.

Monod, A. and Doussin, J.: Structure-activity relationship for the estimation of OH-oxidation rate constants of aliphatic organic compounds in the aqueous phase: alkanes, alcohols, organic acids and bases, Atmospheric Environment, 42, 7611–7622, https://doi.org/10.1016/j.atmosenv.2008.06.005, 2008.

Mouchel-Vallon, C., Deguillaume, L., Monod, A., Perroux, H., Rose, C., Ghigo, G., Long, Y., Leriche, M., Aumont, B., Patryl, L., et al.: CLEPS 1.0: A new protocol for cloud aqueous phase oxidation of VOC mechanisms, Geoscientific Model Development, 10, 1339–1362, https://doi.org/10.5194/gmd-10-1339-2017, 2017.

Nguyen, T., Petters, M., Suda, S., Guo, H., Weber, R., and Carlton, A.: Trends in particle-phase liquid water during the Southern Oxidant and Aerosol Study, Atmospheric Chemistry and Physics, 14, 10 911–10 930, 2014.

Novelli, A., Vereecken, L., Bohn, B., Dorn, H.-P., Gkatzelis, G. I., Hofzumahaus, A., Holland, F., Reimer, D., Rohrer, F., Rosanka, S., Taraborrelli, D., Tillmann, R., Wegener, R., Yu, Z., Kiendler-Scharr, A., Wahner, A., and Fuchs, H.: Importance of isomerization reactions for OH radical regeneration from the photo-oxidation of isoprene investigated in the atmospheric simulation chamber SAPHIR, Atmospheric Chemistry and Physics, 20, 3333–3355, https://doi.org/10.5194/acp-20-3333-2020, publisher: Copernicus GmbH, 2020.

Novelli, A., Cho, C., Fuchs, H., Hofzumahaus, A., Rohrer, F., Tillmann, R., Kiendler-Scharr, A., Wahner, A., and Vereecken, L.: Experimental and theoretical study on the impact of a nitrate group on the chemistry of alkoxy radicals, Physical Chemistry Chemical Physics, 23, 5474–5495, 2021.

Nölscher, A. C., Butler, T., Auld, J., Veres, P., Muñoz, A., Taraborrelli, D., Vereecken, L., Lelieveld, J., and Williams, J.: Using total OH reactivity to assess isoprene photooxidation via measurement and model, Atmospheric Environment, 89, 453–463, https://doi.org/10.1016/j.atmosenv.2014.02.024, 2014.

Octaviani, M., Shrivastava, M., Zaveri, R. A., Zelenyuk, A., Zhang, Y., Rasool, Q. Z., Bell, D. M., Riva, M., Glasius, M., and Surratt, J. D.: Modeling the Size Distribution and Chemical Composition of Secondary Organic Aerosols during the Reactive Uptake of Isoprene-Derived Epoxydiols under Low-Humidity Condition, ACS Earth and Space Chemistry, 5, 3247–3257, https://doi.org/10.1021/acsearthspacechem.1c00303, publisher: American Chemical Society, 2021.

Pang, J. Y. S., Novelli, A., Kaminski, M., Acir, I.-H., Bohn, B., Carlsson, P. T. M., Cho, C., Dorn, H.-P., Hofzumahaus, A., Li, X., Lutz, A., Nehr, S., Reimer, D., Rohrer, F., Tillmann, R., Wegener, R., Kiendler-Scharr, A., Wahner, A., and Fuchs, H.: Investigation of the limonene photooxidation by OH at different NO concentrations in the atmospheric simulation chamber SAPHIR (Simulation of Atmospheric PHoto-

chemistry In a large Reaction Chamber), Atmospheric Chemistry and Physics, 22, 8497–8527, https://doi.org/10.5194/acp-22-8497-2022, 2022.

Perring, A. E., Pusede, S. E., and Cohen, R. C.: An Observational Perspective on the Atmospheric Impacts of Alkyl and Multifunctional Nitrates on Ozone and Secondary Organic Aerosol, Chemical Reviews, 113, 5848–5870, https://doi.org/10.1021/cr300520x, publisher: American Chemical Society, 2013.

Petters, S. S., Cui, T., Zhang, Z., Gold, A., McNeill, V. F., Surratt, J. D., and Turpin, B. J.: Organosulfates from Dark Aqueous Reactions of Isoprene-Derived Epoxydiols Under Cloud and Fog Conditions: Kinetics, Mechanism, and Effect of Reaction Environment on Regioselectivity of Sulfate Addition, ACS Earth and Space Chemistry, 5, 474–486, https://doi.org/10.1021/acsearthspacechem.0c00293?ref=pdf, 2021.

Pozzer, A., Reifenberg, S. F., Kumar, V., Franco, B., Kohl, M., Taraborrelli, D., Gromov, S., Ehrhart, S., Jöckel, P., Sander, R., Fall, V., Rosanka, S., Karydis, V., Akritidis, D., Emmerichs, T., Crippa, M., Guizzardi, D., Kaiser, J. W., Clarisse, L., Kiendler-Scharr, A., Tost, H., and Tsimpidi, A.: Simulation of organics in the atmosphere: evaluation of EMACv2.54 with the Mainz Organic Mechanism (MOM) coupled to the ORACLE (v1.0) submodel, Geoscientific Model Development, 15, 2673–2710, https://doi.org/10.5194/gmd-15-2673-2022, publisher: Copernicus GmbH, 2022.

Pringle, K. J., Tost, H., Message, S., Steil, B., Giannadaki, D., Nenes, A., Fountoukis, C., Stier, P., Vignati, E., and Lelieveld, J.: Description and evaluation of GMXe: a new aerosol submodel for global simulations (v1), Geoscientific Model Development, 3, 391–412, https://doi.org/10.5194/gmd-3-391-2010, publisher: Copernicus GmbH, 2010.

Pye, H., Chan, A., Barkley, M., and Seinfeld, J.: Global modeling of organic aerosol: the importance of reactive nitrogen (NO x and NO 3), Atmospheric Chemistry and Physics, 10, 11 261–11 276, https://doi.org/10.5194/acp-10-11261-2010, 2010.

Raventos-Duran, T., Camredon, M., Valorso, R., Mouchel-Vallon, C., and Aumont, B.: Structure-activity relationships to estimate the effective Henry's law constants of organics of atmospheric interest, Atmospheric Chemistry and Physics, 10, 7643–7654, https://doi.org/10.5194/acp-10-7643-2010, 2010.

Riedel, T., Lin, Y.-H., Zhang, Z., Chu, K., Thornton, J., Vizuete, W., Gold, A., and Surratt, J.: Constraining condensed-phase formation kinetics of secondary organic aerosol components from isoprene epoxydiols, Atmospheric Chemistry and Physics, 16, 1245–1254, https://doi.org/10.5194/acp-16-1245-2016, 2016.

Rohrer, F., Bohn, B., Brauers, T., Brüning, D., Johnen, F.-J., Wahner, A., and Kleffmann, J.: Characterisation of the photolytic HONO-source in the atmosphere simulation chamber SAPHIR, Atmospheric Chemistry and Physics, 5, 2189–2201, 2005.

Rosanka, S., Sander, R., Wahner, A., and Taraborrelli, D.: Oxidation of low-molecular-weight organic compounds in cloud droplets: development of the Jülich Aqueous-phase Mechanism of Organic Chemistry (JAMOC) in CAABA/MECCA (version 4.5. 0), Geoscientific Model Development, 14, 4103–4115, https://doi.org/10.5194/gmd-2020-337, 2021.

Rosanka, S., Tost, H., Sander, R., Jöckel, P., Kerkweg, A., and Taraborrelli, D.: How non-equilibrium aerosol chemistry impacts particle acidity: the GMXe AERosol CHEMistry (GMXe–AERCHEM, v1.0) sub-submodel of MESSy, EGUsphere, pp. 1–29, https://doi.org/10.5194/egusphere-2023-2587, publisher: Copernicus GmbH, 2023.

Ryder, O. S., Campbell, N. R., Shaloski, M., Al-Mashat, H., Nathanson, G. M., and Bertram, T. H.: Role of Organics in Regulating ClNO2 Production at the Air–Sea Interface, The Journal of Physical Chemistry A, 119, 8519–8526, https://doi.org/10.1021/jp5129673, publisher: American Chemical Society, 2015.

Sanchez, D., Jeong, D., Seco, R., Wrangham, I., Park, J.-H., Brune, W. H., Koss, A., Gilman, J., de Gouw, J., Misztal, P., et al.: Intercomparison of OH and OH reactivity measurements in a high isoprene and low NO environment during the Southern Oxidant and Aerosol Study (SOAS), Atmospheric Environment, 174, 227–236, 2018.

Sander, R.: Compilation of Henry's law constants (version 4.0) for water as solvent, Atmospheric Chemistry and Physics, 15, 4399–4981, https://doi.org/10.5194/acp-15-4399-2015, 2015.

Sander, R.: Compilation of Henry's law constants (version 5.0.0) for water as solvent, 23, 10 901–12 440, https://doi.org/10.5194/ACP-23-10901-2023, 2023.

Sander, R., Kerkweg, A., Jöckel, P., and Lelieveld, J.: Technical note: The new comprehensive atmospheric chemistry module MECCA, Atmos. Chem. Phys., 5, 445–450, https://doi.org/10.5194/ACP-5-445-2005, 2005.

Sander, R., Baumgaertner, A., Gromov, S., Harder, H., Jöckel, P., Kerkweg, A., Kubistin, D., Regelin, E., Riede, H., Sandu, A., et al.: The atmospheric chemistry box model CAABA/MECCA-3.0, Geoscientific Model Development, 4, 373–380, https://doi.org/10.5194/gmd-4-373-2011, 2011.

Sander, R., Jöckel, P., Kirner, O., Kunert, A. T., Landgraf, J., and Pozzer, A.: The photolysis module JVAL-14, compatible with the MESSy standard, and the JVal PreProcessor (JVPP), Geosci. Model Dev., 7, 2653–2662, https://doi.org/10.5194/GMD-7-2653-2014, 2014.

Sander, R., Baumgaertner, A., Cabrera-Perez, D., Frank, F., Gromov, S., Grooß, J.-U., Harder, H., Huijnen, V., Jöckel, P., Karydis, V. A., et al.: The community atmospheric chemistry box model CAABA/MECCA-4.0, Geoscientific model development, 12, 1365–1385, https://doi.org/10.5194/gmd-12-1365-2019, 2019.

Sareen, N., Carlton, A. G., Surratt, J. D., Gold, A., Lee, B., Lopez-Hilfiker, F. D., Mohr, C., Thornton, J. A., Zhang, Z., Lim, Y. B., et al.: Identifying precursors and aqueous organic aerosol formation pathways during the SOAS campaign, Atmospheric Chemistry and Physics, 16, 14 409–14 420, 2016.

Schervish, M. and Donahue, N. M.: Peroxy radical chemistry and the volatility basis set, Atmospheric Chemistry and Physics, 20, 1183–1199, https://doi.org/10.5194/acp-20-1183-2020, 2020.

Schervish, M. and Donahue, N. M.: Peroxy radical kinetics and new particle formation, Environmental Science: Atmospheres, 1, 79–92, 2021.

Schlosser, E., Bohn, B., Brauers, T., Dorn, H.-P., Fuchs, H., Häseler, R., Hofzumahaus, A., Holland, F., Rohrer, F., Rupp, L. O., et al.: Intercomparison of two hydroxyl radical measurement techniques at the atmosphere simulation chamber SAPHIR, Journal of atmospheric chemistry, 56, 187–205, 2007.

Schmitt, S.: Formation of Secondary Organic Aerosol from Photo-Oxidation of Benzene: a Chamber Study, vol. 412, 2018.

Seinfeld, J. H. and Pandis, S. N.: Atmospheric chemistry and physics: from air pollution to climate change, John Wiley & Sons, 2016.

Shrivastava, M., Cappa, C. D., Fan, J., Goldstein, A. H., Guenther, A. B., Jimenez, J. L., Kuang, C., Laskin, A., Martin, S. T., Ng, N. L., et al.: Recent advances in understanding secondary organic aerosol: Implications for global climate forcing, Reviews of Geophysics, 55, 509–559, 2017.

Sivaramakrishnan, R. and Michael, J.: Rate constants for OH with selected large alkanes: shock-tube measurements and an improved group scheme, The Journal of Physical Chemistry A, 113, 5047–5060, https://doi.org/10.1021/jp810987u, 2009.

Soni, M., Sander, R., Sahu, L. K., Taraborrelli, D., Liu, P., Patel, A., Girach, I. A., Pozzer, A., Gunthe, S. S., and Ojha, N.: Comprehensive multiphase chlorine chemistry in the box model CAABA/MECCA: Implications to atmospheric oxidative capacity, EGUsphere, 2023, 1–24, https://doi.org/10.5194/egusphere-2023-652, 2023.

St. Clair, J. M., Rivera-Rios, J. C., Crounse, J. D., Knap, H. C., Bates, K. H., Teng, A. P., Jørgensen, S., Kjaergaard, H. G., Keutsch, F. N., and Wennberg, P. O.: Kinetics and products of the reaction of the first-generation isoprene hydroxy hydroperoxide (ISOPOOH) with OH, The Journal of Physical Chemistry A, 120, 1441–1451, https://doi.org/10.1021/acs.jpca.5b06532, 2016.

Staudinger, J. and Roberts, P. V.: A critical compilation of Henry's law constant temperature dependence relations for organic compounds in dilute aqueous solutions, Chemosphere, 44, 561–576, https://doi.org/10.1016/S0045-6535(00)00505-1, 2001.

Staudt, S., Gord, J. R., Karimova, N. V., McDuffie, E. E., Brown, S. S., Gerber, R. B., Nathanson, G. M., and Bertram, T. H.: Sulfate and Carboxylate Suppress the Formation of ClNO2 at Atmospheric Interfaces, ACS Earth and Space Chemistry, 3, 1987–1997, https://doi.org/10.1021/acsearthspacechem.9b00177, publisher: American Chemical Society, 2019.

Subramani, M., Saravanan, V., Theerthagiri, J., Subramaniam, V., Pazhanivel, T., Ramasamy, S., and Manickam, S.: Kinetics and degradation of camphene with OH radicals and its subsequent fate under the atmospheric O2 and NO radicals-A theoretical study, Chemosphere, 267, 129 250, 2021.

Taraborrelli, D., Lawrence, M. G., Crowley, J. N., Dillon, T. J., Gromov, S., Groß, C. B. M., Vereecken, L., and Lelieveld, J.: Hydroxyl radical buffered by isoprene oxidation over tropical forests, Nature Geoscience, 5, 190–193, https://doi.org/10.1038/ngeo1405, number: 3 Publisher: Nature Publishing Group, 2012.

Taraborrelli, D., Cabrera-Perez, D., Bacer, S., Gromov, S., Lelieveld, J., Sander, R., and Pozzer, A.: Influence of aromatics on tropospheric gas-phase composition, Atmospheric Chemistry and Physics, 21, 2615–2636, https://doi.org/10.5194/acp-21-2615-2021, publisher: Copernicus GmbH, 2021.

Teng, A. P., Crounse, J. D., Lee, L., St. Clair, J. M., Cohen, R. C., and Wennberg, P. O.: Hydroxy nitrate production in the OH-initiated oxidation of alkenes, Atmospheric Chemistry and Physics, 15, 4297–4316, https://doi.org/10.5194/acp-15-4297-2015, publisher: Copernicus GmbH, 2015.

Tilmes, S., Hodzic, A., Emmons, L., Mills, M., Gettelman, A., Kinnison, D. E., Park, M., Lamarque, J.-F., Vitt, F., Shrivastava, M., et al.: Climate forcing and trends of organic aerosols in the Community Earth System Model (CESM2), Journal of Advances in Modeling Earth Systems, 11, 4323–4351, 2019.

Tost, H., Jöckel, P., Kerkweg, A., Sander, R., and Lelieveld, J.: A new comprehensive SCAVenging submodel for global atmospheric chemistry modelling, Atmospheric Chemistry and Physics, 6, 565–574, 2006.

Tsimpidi, A., Karydis, V., Pozzer, A., Pandis, S., and Lelieveld, J.: ORACLE (v1. 0): module to simulate the organic aerosol composition and evolution in the atmosphere, Geoscientific Model Development, 7, 3153–3172, 2014.

US-EPA: Estimation Programs Interface Suite™ for Microsoft® Windows, v 4.11, united States Environmental Protection Agency, Washington, DC, USA, 2012.

Vasquez, K. T., Crounse, J. D., Schulze, B. C., Bates, K. H., Teng, A. P., Xu, L., Allen, H. M., and Wennberg, P. O.: Rapid hydrolysis of tertiary isoprene nitrate efficiently removes NO_x from the atmosphere, Proc. Nat. Acad. Sci. USA, 117, 33 011–33 016, https://doi.org/10.1073/pnas.2017442117, 2020.

Vereecken, L.: Reaction mechanisms for the atmospheric oxidation of monocyclic aromatic compounds, in: Advances in Atmospheric Chemistry: Volume 2: Organic Oxidation and Multiphase Chemistry, pp. 377–527, World Scientific, 2019.

Vereecken, L. and Nozière, B.: H migration in peroxy radicals under atmospheric conditions, Atmospheric chemistry and physics, 20, 7429–7458, https://doi.org/10.5194/acp-20-7429-2020, 2020.

Vereecken, L. and Peeters, J.: A theoretical study of the OH-initiated gas-phase oxidation mechanism of β-pinene (C 10 H 16): first generation products, Physical Chemistry Chemical Physics, 14, 3802–3815, https://doi.org/10.1039/c2cp23711c, 2012.

Vereecken, L., Carlsson, P., Novelli, A., Bernard, F., Brown, S., Cho, C., Crowley, J., Fuchs, H., Mellouki, W., Reimer, D., et al.: Theoretical and experimental study of peroxy and alkoxy radicals in the NO 3-initiated oxidation of isoprene, Physical Chemistry Chemical Physics, 23, 5496–5515, https://doi.org/10.1039/D0CP06267G, 2021.

Wang, C., Yuan, T., Wood, S. A., Goss, K.-U., Li, J., Ying, Q., and Wania, F.: Uncertain Henry's law constants compromise equilibrium partitioning calculations of atmospheric oxidation products, Atmospheric Chemistry and Physics, 17, 7529–7540, https://doi.org/10.5194/acp-17-7529-2017, 2017.

Wang, L., Wu, R., and Xu, C.: Atmospheric oxidation mechanism of benzene. Fates of alkoxy radical intermediates and revised mechanism, The Journal of Physical Chemistry A, 117, 14 163–14 168, https://doi.org/10.1021/jp4101762, 2013.

Wennberg, P. O., Bates, K. H., Crounse, J. D., Dodson, L. G., McVay, R. C., Mertens, L. A., Nguyen, T. B., Praske, E., Schwantes, R. H., Smarte, M. D., et al.: Gas-phase reactions of isoprene and its major oxidation products, Chemical reviews, 118, 3337–3390, https://doi.org/10.1021/acs.chemrev.7b00439, 2018.

Wu, R., Pan, S., Li, Y., and Wang, L.: Atmospheric oxidation mechanism of toluene, The Journal of Physical Chemistry A, 118, 4533–4547, 2014.

Wu, X., Huang, C., Chai, J., and Zhang, F.: Formation of Substituted Alkyls as Precursors of Peroxy Radicals with a Rapid H-Shift in the Atmosphere, The Journal of Physical Chemistry Letters, 12, 8790–8797, https://doi.org/10.1021/acs.jpclett.1c02503, 2021.

Xu, J., Griffin, R. J., Liu, Y., Nakao, S., and Cocker III, D. R.: Simulated impact of NOx on SOA formation from oxidation of toluene and m-xylene, Atmospheric Environment, 101, 217–225, https://doi.org/10.1016/j.atmosenv.2014.11.008, 2015a.

Xu, L., Suresh, S., Guo, H., Weber, R. J., and Ng, N. L.: Aerosol characterization over the southeastern United States using high-resolution aerosol mass spectrometry: spatial and seasonal variation of aerosol composition and sources with a focus on organic nitrates, Atmospheric Chemistry and Physics, 15, 7307–7336, https://doi.org/10.5194/acp-15-7307-2015, 2015b.

Xu, L., Møller, K. H., Crounse, J. D., Kjaergaard, H. G., and Wennberg, P. O.: New insights into the radical chemistry and product distribution in the OH-initiated oxidation of benzene, Environmental Science & Technology, 54, 13 467–13 477, https://doi.org/10.1021/acs.est.0c04780, 2020.

You, Y., Kanawade, V., De Gouw, J., Guenther, A. B., Madronich, S., Sierra-Hernández, M., Lawler, M., Smith, J. N., Takahama, S., Ruggeri, G., et al.: Atmospheric amines and ammonia measured with a chemical ionization mass spectrometer (CIMS), Atmospheric Chemistry and Physics, 14, 12 181–12 194, 2014.

Zaytsev, A., Koss, A. R., Breitenlechner, M., Krechmer, J. E., Nihill, K. J., Lim, C. Y., Rowe, J. C., Cox, J. L., Moss, J., Roscioli, J. R., et al.: Mechanistic study of the formation of ring-retaining and ring-opening products from the oxidation of aromatic compounds under urban atmospheric conditions, Atmos. Chem. Phys, 19, 15 117–15 129, 2019.

Zhang, Y., Chen, Y., Lambe, A. T., Olson, N. E., Lei, Z., Craig, R. L., Zhang, Z., Gold, A., Onasch, T. B., Jayne, J. T., Worsnop, D. R., Gaston, C. J., Thornton, J. A., Vizuete, W., Ault, A. P., and Surratt, J. D.: Effect of the Aerosol-Phase State on Secondary Organic Aerosol Formation from the Reactive Uptake of Isoprene-Derived Epoxydiols (IEPOX), Environmental Science & Technology Letters, 5, 167–174, https://doi.org/10.1021/acs.estlett.8b00044, publisher: American Chemical Society, 2018.

Zhong, M. and Jang, M.: Light absorption coefficient measurement of SOA using a UV–Visible spectrometer connected with an integrating sphere, Atmospheric environment, 45, 4263–4271, https://doi.org/10.1016/j.atmosenv.2011.04.082, 2011.

Zhu, J., Penner, J. E., Lin, G., Zhou, C., Xu, L., and Zhuang, B.: Mechanism of SOA formation determines magnitude of radiative effects, Proceedings of the National Academy of Sciences, 114, 12 685–12 690, https://doi.org/10.1073/pnas.1712273114, 2017.